A New Generalized Karplus-Type Equation Relating Vicinal Proton-Fluorine Coupling Constants to H−C−C−F Torsion Angles

Christophe Thibaudeau,[†] Janez Plavec,*[,‡] and Jyoti Chattopadhyaya*[,†,§]

Department of Bioorganic Chemistry, Box 581, Biomedical Center, University of Uppsala, S-751 23 Uppsala, Sweden, and National Institute of Chemistry, Hajdrihova 19, SI-1115 Ljubljana, Slovenia

Received January 27, 1998

A new seven-parameter Karplus-type relation between vicinal proton−fluorine coupling constants and the corresponding H−C−C−F torsion angles has been developed. The optimum values of the seven parameters were determined using a data set consisting of 57 $^3J_{HF}$ values and the corresponding Φ_{HF} torsion angles (ranging from cis, gauche, and trans regions) based upon ab initio structures as well as on the conformational analysis of temperature-dependent $^3J_{HH}$ of monofluorinated nucleosides **1**−**11**, which were also complemented with the data from conformationally fixed compounds **12**−**22**. The best fit generalized Karplus-type equation shows the difference between input and back-calculated $^3J_{HF}$ below 2.9 Hz with the overall rms deviation of 1.38 Hz, amounting to a total of 4% error for transoid coupling of ≈40−46 Hz, which compares very well with about 5% error encountered earlier in the experimental and the back-calculated $^3J_{HH}$ of 8−9 Hz in the latest Karplus−Altona equation (ref 14). This is the first use of a new Karplus-type equation correlating $^3J_{HF}$ with the H−C−C−F torsion angle in a quantitative manner (by making use of correction terms for substituent electronegativity as well as for H−C−C and F−C−C bond angles) to explore the pseudorotational equilibria of monofluorinated nucleosides **24** and **25** as well as difluorinated nucleosides **26**−**29** with the use of both $^3J_{HH}$ and $^3J_{HF}$ coupling constants in an iterative manner. The use of temperature-dependent $^3J_{HF}$ in combination with $^3J_{HH}$ greatly facilitates the conformational analysis of fluorinated sugar moieties of nucleosides because of the overwhelming increase of the number of experimental data points over the unknowns defining the pseudorotational equilibrium. This enables the pseudorotational parameters *P* and Ψ_m of the two interconverting conformers to be more accurately defined. The best use of our new generalized Karplus-type relation is that it enables solution structure determination of fluorinated nucleosides or any other fluorinated compounds in which the number of measurable vicinal proton−proton couplings are not adequate enough to fully define the geometry of the system as in difluorinated nucleosides **26**−**29**.

Introduction

Fluorinated compounds[1] are widely used in biochemistry, medicinal chemistry, and pharmacology. Much effort has been devoted to synthesize various fluorinated nucleoside analogues, which are widely employed as experimental antitumor and antiviral agents. Most of the 2′-fluoronucleosides exhibit biological activity after being 5′-triphosphorylated enzymatically by kinases of various origins.[2] Introduction of a fluorine atom at a sugar carbon in nucleosides alters their biological activities toward various cellular, pathogenic, and tumor-specific enzymes in various ways. These enzymes include deaminases, kinases, DNA polymerases, ribonucleotide reductase, or thymidylate synthetase.[2] The replacement of a hydroxy group by a fluorine atom causes only a minor change in the steric effect of the functionality, but such a substitution has profound effects on the chemical properties as well as on the stereoelectronic properties, which result in specific overall conformational change of the fluorinated nucleosides: (i) The glycosyl bond is strengthened resisting enzymatic hydrolysis by phosphorylases.[2] (ii) The fluorine atom is strongly electron-withdrawing, and its atomic size is between that of a proton and a hydroxyl group; hence the gauche effect of 2″-F, for example, in 2′-fluorinated-2′-deoxy nucleoside drives the sugar conformation in a way that resembles RNA more than DNA.[3] (iii) The stronger gauche effect of the fluorine substituent due to its high electronegativity has a profound stereoelectronic effect on the stereochemical orientation of the neighboring groups; thereby the fluorine substituent governs the overall conformation of the sugar ring.[3−6] For example it has been recently noted by Marquez et al.[7] that 2′-fluorothymidine in the *ara* configuration takes up the North-type conformation, whereas 2″-fluoro-thymidine in the *ribo* configuration puckers preferentially in the South-type conformation to further stabilize Dickerson-Drew dodecamer, which means that the strength of the fluorine-

† Biomedical Center.
‡ National Institute of Chemistry.
§ E-mail: jyoti@bioorgchem.uu.se. Fax: +4618-554495. Web site: http://bioorgchem.boc.uu.se/.

(1) Welch, J. T.; Eswarakrishnan, S. *Fluorine in Bioorganic Chemistry*; John Wiley and Sons: New York, 1991, p 261.
(2) Tsuchiya, T. *Adv. Carbohydr. Chem. Biochem.* **1990**, *48*, 91.
(3) Uesugi, S.; Kaneyasu, T.; Imura, J.; Ikehara, M.; Kan, S.; Ts'O, P. O. P. *Biopolymers* **1983**, *22*, 1189.
(4) Cheng, D. M.; Kan, L.-S.; Ts'O, P. O. P.; Takatsuka, Y.; Ikehara, M. *Biopolymers* **1983**, *22*, 1427.
(5) Van der Boogaart, J. E.; Kalinichenko, E. N.; Podkopaeva, T. L.; Mikhailopulo, I. A.; Altona, C. *Eur. J. Biochem.* **1994**, *221*, 759.
(6) Guschlbauer, W.; Jankowski, K. *Nucleic Acids Res.* **1980**, *8*, 1421.
(7) Marquez, V. E. Personal communication.

S0022-3263(98)00144-3 CCC: $15.00
Published on Web 07/07/1998

Scheme 1. $^3J_{HF}$ of Compounds 1−17 Used for the Parametrization of Karplus Equation (3) (Sections C−G)

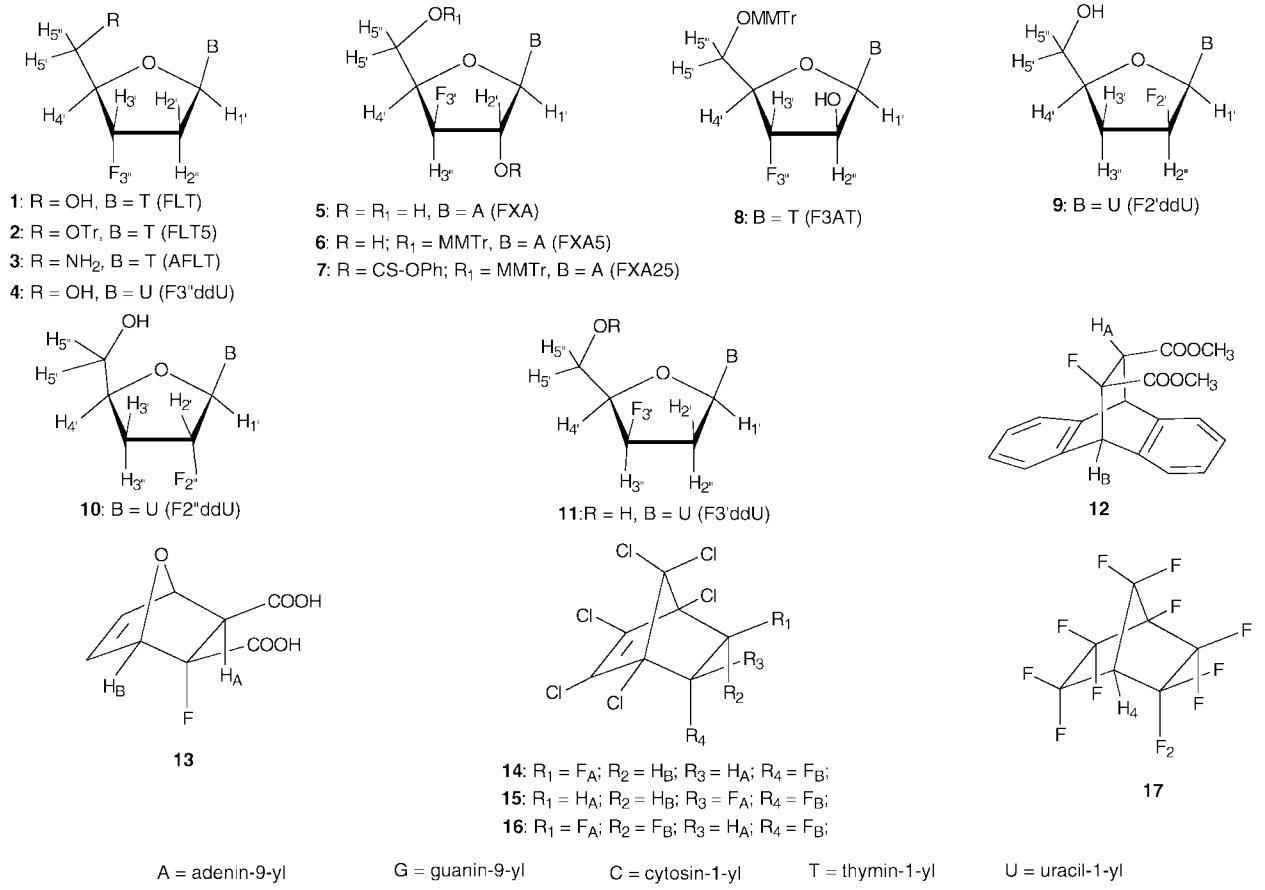

induced gauche effect that determines the overall conformation of the sugar ring is configuration-dependent.

This suggests that there should be a dependable way to define the conformation and the conformational equilibria in solution for the sugar-fluorinated nucleosides using NMR methods in order to correlate their structure−activity relationships, both in the presence and in the absence of target enzymes.

Use of experimental NMR data in the conformational or structural analysis consists of the measurement of NOEs and coupling constants.[8] The most interesting aspect of $^3J_{HH}$ proton−proton as well as heteronuclear coupling constants is undoubtedly their dependence on the torsion angles. $^3J_{HF}$ coupling constants have been *qualitatively* used[9] in the conformational analysis of fluorinated sugars, nucleosides, and other organic molecules assuming simple three-parameter relations such as $^3J_{HF} = A \cos^2 \Phi_{HF} + B \cos \Phi_{HF} + C$, where Φ_{HF} is the H−C−C−F torsion angle. It has been discussed that vicinal proton−fluorine coupling constants depend on the torsion angle, on the electronegativity of the other substituents of the system, and on the bond angle changes.[9c,10a−d] It has been also suggested that $^3J_{HF}$ values depend linearly on the electronegativity of the substituents on the vicinal carbon atoms.[10e] While trying to make use of these suggestions, we have realized that the quantitation of the effect of the fluorine substituent in the form of a suitable Karplus equation is far more complicated than what has been addressed before. Hence, we have searched for more elaborate expressions which would correlate the experimental set of $^3J_{HF}$ and H−C−C−F torsion angles in a more satisfactory and quantitative manner. Altona et al. have successfully proposed a six-parameter relationship correlating $^3J_{HH}$ and H−C−C−H torsion angle, which includes a correction term for the substituent electronegativity, H−C−C−H torsion angle, and the relative orientations of the substituents.[11] We herein have used this Altona's work as the basis for the formulation of a new Karplus equation for a quantitative correlation of $^3J_{HF}$ coupling constants with the corresponding H−C−C−F torsion angles by introducing a correction term for the fluorine substitution effect on the H−C−C−F coupling pathway as well on the F−C−C and H−C−C bond angle changes (Schemes 1 and 2).[12]

Results

Our strategy has been to construct a data set of $^3J_{HF}$ coupling constants and the corresponding Φ_{HCCF} torsion

(8) For a recent review, see the contributions in *Magn. Reson. Chem.* **1996**, *34*, S1−S186.

(9) (a) Cushley, R. J.; Codington, J. F.; Fox, J. J. *Can. J. Chem.* **1967**, *46*, 1131. (b) Lipnick, R. L.; Fissekis, J. D. *Biochim. Biophys. Acta* **1980**, *608*, 96. (c) Phillips, L.; Wray, V. *J. Chem. Soc. (B)* **1971**, 1618. (d) Hall, L. D.; Manville, J. F. *Chem. Commun.* **1968**, 37. (e) Foster, A. B.; Hems, R.; Hall, L. D. *Can. J. Chem.* **1970**, *48*, 3937.

(10) (a) Williamson, K. L.; Li Hsu, Y.-F.; Hall, F. H.; Swager, S.; Coulter, M. *J. Am. Chem. Soc.* **1968**, *90*, 6717. (b) Ihrig, A. M.; Smith, S. L. *J. Am. Chem. Soc.* **1970**, *92*, 759. (c) Gopinathan, M. S.; Narasimhan, P. T. *Mol. Phys.* **1971**, *21*, 1144. (d) Govil, G. *Mol. Phys.* **1971**, *21*, 953. (e) Abraham R. J.; Cavalli, L. *Mol. Phys.* **1965**, *9*, 67. (f) Emsley, J. W.; Phillips, L.; Wray, V. Fluorine Coupling Constants. In *Progress in Nuclear Magnetic Resonance Spectroscopy*; Emsley, J. W., Feeney, J., Sutcliffe, L. H., Eds.; Pergamon Press: New York, 1977; Vol. 10(3/4), pp 229.

(11) Haasnoot, C. A. G.; de Leeuw, F. A. A. M.; Altona, C. *Tetrahedron* **1980**, *36*, 2783.

(12) (a) Karplus, M. *J. Am. Chem. Soc.* **1963**, *85*, 2870. (b) Imai, K.; Osawa, E. *Magn. Reson. Chem.* **1990**, *28*, 668.

Scheme 2. $^3J_{HF}$ of Compounds 18−23 Used for Parametrization of Karplus Equation (3) (Sections C−G) and $^3J_{HF}$ of Compounds 24−29 Where Newly Parametrized Karplus Equation (3) is applied (Sections C−G)

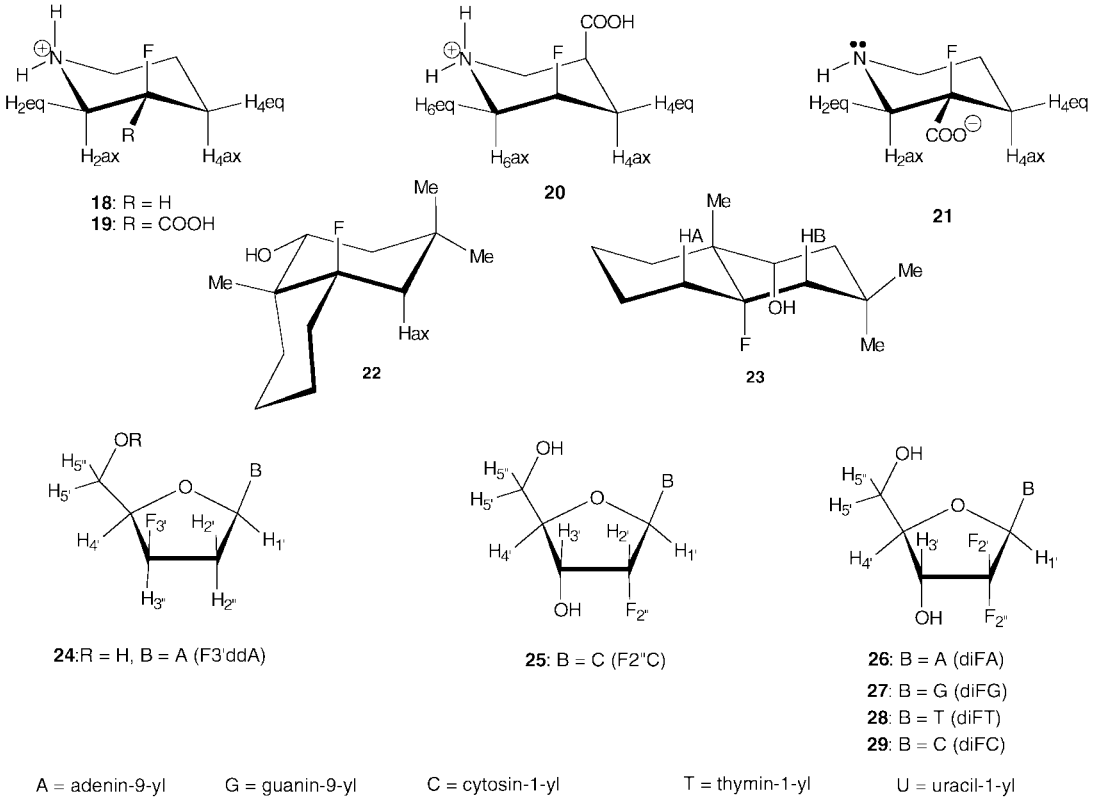

angles based upon ab initio optimized structures (to get *A* and *B* parameters, vide infra) and on the proton−proton conformational analysis of monofluorinated nucleosides[13] **1**−**11** using the PSEUROT program.[14] The resulting $^3J_{HF} - \Phi_{HCCF}$ data set was used for the evaluation of our trial Karplus-type equations. During the iterative procedure (Scheme 3) we have utilized the literature data[10a,b,f,21,22] on conformationally constrained compounds **12**−**22** that show fixed H−C−C−F torsion angles in the ranges that were not covered by the conformational analysis of nucleosides **1**−**11** (in particular Φ_{HCCF} around 90°, see below).

Our Karplus-type equation that best fits the experimental data was used to explore the pseudorotational equilibria of monoflurinated nucleosides **24**−**25** as well as difluorinated nucleosides **26**−**29** with the use of both experimental $^3J_{HH}$ and experimental $^3J_{HF}$ coupling constants. Note that compounds **26**−**29** are known important anticancer[2] compounds, and their solution conformational analysis based on a single available proton−proton coupling constant (i.e., $^3J_{H3'H4'}$) is at best misleading. Here, it was crystal clear that the use of both proton−fluorine and proton−proton coupling constants is the only way to perform a dependable conformational analysis of their sugar moieties.

(A) Pseudorotation of the Pentose Sugar Moiety in DNA and RNA. According to the pseudorotation concept the cyclopentane ring is involved in continuous interconversions of puckered forms.[15] The puckering mode can be defined by using puckering parameters based on the deviation of the endocyclic torsion angles from 0. The Altona-Sundaralingam parameters[16] are the phase angle of pseudorotation (*P*) and the puckering amplitude (Ψ_m). *P* defines the part of the ring which is most puckered, and Ψ_m indicates the extent of the puckering. The pseudorotation cycle, in which *P* varies from 0° to 360° through a set of twenty distinct twist and envelope conformations, can be subdivided into north ($P \approx 0°$), east ($P \approx 90°$), south ($P \approx 180°$), and west ($P \approx 270°$) regions. In a survey of X-ray crystal structures[17] of nucleosides and nucleotides, sugar moieties were found both in North (N) and South (S) conformations. The former range ($0° < P < 36°$) is centered around $P = 18°$ (C3′-*endo*), whereas the latter ($144° < P < 180°$) is centered around $P = 162°$ (C2′-*endo*). However, there are also a few examples of X-ray structures[17] which have sugar conformations in the east (E) region, which supports the hypothesis that the N ⇄ S interconversion proceeds through the E, rather than the west (W) conformation. The values of Ψ_m were found in a range from 30° to 46°. The hypothesis of the two-state dynamic N ⇄ S pseudorotational equilibrium (Scheme 4) in nucleosides and nucleotides in solution was originally mainly based on statistical distributions of X-ray crystal structures.[17] However, it has also been experimentally evidenced by several NMR studies in aqueous solution:

(13) Barchi, J. J.; Jeong, L.-S.; Siddiqui, M. A.; Marquez, V. E. *J. Biochem. Biophys. Methods* **1997**, *34*, 11.

(14) (a) De Leeuw, F. A. A. M.; Altona, C. *J. Comput. Chem.* **1983**, *4*, 428, and PSEUROT, QCPE program No 463. (b) Diez, E.; Fabian, J. S.; Guilleme, J.; Altona, C.; Donders, L. A. *Mol. Phys.* **1989**, *68*, 49. (c) Donders, L. A.; de Leeuw, F. A. A. M.; Altona, C. *Magn. Reson. Chem.* **1989**, *27*, 556. (d) Altona, C.; Ippel, J. H.; Hoekzema, A. J. A. W.; Erkelens, C.; Groesbeek, G.; Donders, L. A. *Magn. Reson. Chem.* **1989**, *27*, 564.

(15) Kilpatrick, J. E.; Pitzer, K. S.; Spitzer, R. *J. Am. Chem. Soc.* **1947**, *64*, 2483.

(16) Altona, C.; Sundaralingam, M. *J. Am. Chem. Soc.* **1972**, *94*, 8205. *Ibid.* **1973**, *95*, 2333.

(17) de Leeuw, H. P. M.; Haasnoot, C. A. G.; Altona, C. *Isr. J. Chem.* **1980**, *20*, 108.

Scheme 3. PSEUROT+J_{HF} Program

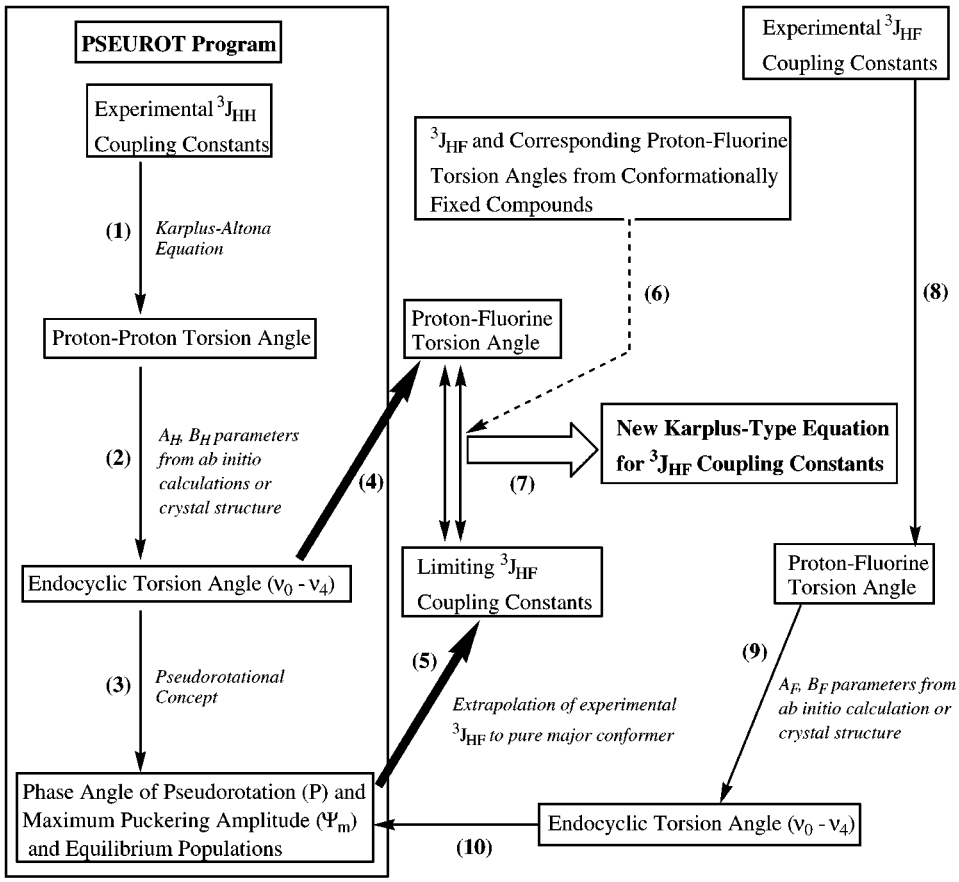

Scheme 4

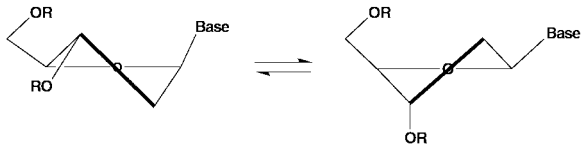

North sugar (C_3-*endo*-C_2-*exo*)
Phase angle (P) = 0° ≤ P ≤ 36°;
Puckering amplitude (Ψ_m) = 38.6° ± 3°

South sugar (C_2-*endo*-C_3-*exo*)
Phase angle (P) = 144° ≤ P ≤ 190°;
Puckering amplitude (Ψ_m) = 38.6° ± 3°

Base = adenine-9-yl (A), guanine-9-yl (G), cytosine-1-yl (C), thymine-1-yl (T)
R = H or an internucleotidyl-(3′ → 5′)-phosphodiester moiety in DNA

The two-state N⇄ S pseudorotational equilibrium in nucleosides and nucleotides.

(i) We have recently found that the inflection point of the sigmoidal plots of the pD-dependent thermodynamics of the two-state N ⇄ S pseudorotational equilibrium in β-D-2′,3′-dideoxyribo-,[18t] 2′-deoxyribo-,[18p] and ribonucleosides,[18p] C-nucleosides,[18s] and in some α-D-nucleosides[18t,u] corresponds to the pK_a of the constituent nucleobase, as does the inflection point of the plots of the pD-dependent chemical shift of ^{1}H or ^{13}C of the aglycone. Furthermore, the plot of pH-dependent free energy of the two-state N ⇄ S pseudorotational equilibrium and the pH-dependent proton chemical shift gives a straight line, showing that these two processes are correlated, threreby showing the validity of the concept of the two-state N ⇄ S pseudorotational equilibrium; it also nicely showed that the free energy of the protonation ⇄ deprotonation equilibrium indeed drives the two-state N ⇄ S pseudorotational equilibrium through the tunable stereoelectronic gauche and anomeric effects. (ii) The two-state dynamic N ⇄ S equilibrium has also been further corroborated by the NMR observations of two distinctly identifiable and dynamically interconverting N and S conformations (as evident by their respective chemical shifts and $^3J_{HH}$) of the constituent sugar moieties in oligonucleotides as in B ⇄ Z DNA,[19a,b] A ⇄ Z RNA,[19c,d] or A-form ⇄ B-form lariat RNA.[19e,f]

(B) The Interplay of Stereoelectronic Forces (Gauche and Anomeric Effects) Determines the Overall Sugar Conformation in Nucleosides. The energetics of N ⇄ S conformational equilibrium (Scheme 4) is known to be determined by the relative strengths

(18) (a) Plavec, J.; Tong, W.; Chattopadhyaya, J. *J. Am. Chem. Soc.* **1993**, *115*, 9734. (b) Plavec, J.; Garg, N.; Chattopadhyaya, J. *J. Chem. Soc., Chem. Commun.* **1993**, 1011. (c) Plavec, J.; Koole, L. H.; Chattopadhyaya, J. *J. Biochem. Biophys. Methods* **1992**, *25*, 253. (d) Koole. L. H.; Buck, H. M.; Nyilas, A.; Chattopadhyaya, J. *Can J. Chem.* **1987**, *65*, 2089. (e) Koole, L. H.; Buck, H. M.; Bazin, H.; Chattopadhyaya, J. *Tetrahedron* **1987**, *43*, 2289. (f) Koole, L. H.; Plavec, J.; Liu, H.; Vincent, B. R.; Dyson, M. R.; Coe, P. L.; Walker, R. T.; Hardy, G. W.; Rahim, S. G.; Chattopadhyaya, J. *J. Am. Chem. Soc.* **1992**, *114*, 9934. (g) Plavec, J.; Thibaudeau, C.; Viswanadham, G.; Sund, C.; Chattopadhyaya, J. *J. Chem. Soc., Chem. Commun.* **1994**, 781. (h) Thibaudeau, C.; Plavec, J.; Watanabe, K. A.; Chattopadhyaya, J. *J. Chem. Soc., Chem. Commun.* **1994**, 537. (i) Thibaudeau, C.; Plavec, J.; Garg, N.; Papchikhin, A.; Chattopadhyaya, J. *J. Am. Chem. Soc.* **1994**, *116*, 4038. (j) Plavec, J.; Thibaudeau, C.; Chattopadhyaya, J. *J. Am. Chem. Soc.* **1994**, *116*, 6558. (k) Thibaudeau, C.; Plavec, J.; Chattopadhyaya, J. *J. Am. Chem. Soc.* **1994**, *116*, 8033. (l) Plavec, J. Ph.D. Thesis, Department of Bioorganic Chemistry, Uppsala University, Sweden, 1995. (m) Plavec, J.; Thibaudeau, C.; Chattopadhyaya, J. *Tetrahedron* **1995**, *51*, 11775. (n) Thibaudeau, C.; Plavec, J.; Chattopadhyaya, J. *J. Org. Chem.* **1996**, *61*, 266. (o) Chattopadhyaya, J. *Nucleic Acids Symp. Ser.* **1996**, *35*, 111. (p) Plavec, J.; Thibaudeau, C.; Chattopadhyaya, J. *Pure Appl. Chem.* **1996**, *68*, 2137. (q) Luyten, I.; Thibaudeau, C.; Chattopadhyaya, J. *Tetrahedron* **1997**, *53*, 6433. (r) Thibaudeau, C.; Földesi, A.; Chattopadhyaya, J. *Tetrahedron* **1997**, *53*, 14043. (s) Thibaudeau, C.; Földesi, A.; Chattopadhyaya, J. *Tetrahedron* **1998**, *54*, 1867. (t) Luyten, I.; Thibaudeau, C.; and Chattopadhyaya, J. *J. Org. Chem.* **1997**, *62*, 8800.

of anomeric and gauche effects.[18] The heterocyclic bases are involved in the anomeric effect by orbital mixing of one of the nonbonded lone pairs to the σ^* orbital of the glycosyl bond [i.e., $n(O4') \rightarrow \sigma^*_{C-N}$] to drive the two-state N ⇄ S pseudorotational equilibrium of the constituent β-D-pentofuranosyl moieties.[18p,r,s−v] The anomeric effect in nucleosides is optimal in O4′-*exo* (W) conformation with the pseudoaxial aglycone, but this optimal conformation is unacceptable for steric reasons. The N-type conformation is energetically favored over S-type in terms of the anomeric effect alone, and its strength is closely related to the electronic nature of the aglycone.[18] The protonation of the nucleobase facilitates the $n(O4') \rightarrow \sigma^*_{C-N}$ interactions, thereby resulting in the increased population of N-type conformers.[18p,s−u] The 3′-OH or 3′-OPO_3H^- groups in 2′-deoxynucleos(t)ides drive the N ⇄ S equilibrium toward S-type conformation through the tendency to adopt a gauche orientation of the [O4′−C4′−C3′−O3′] torsion angle.[18h,n] The 2′-OH in ribonucleos(t)ides is involved in three gauche interactions which compete for the drive of N ⇄ S equilibrium: (i) [O4′−C1′−C2′−O2′] drives toward N, (ii) [N1/9−C1′−C2′−O2′] drives toward S, and (iii) [O3′−C3′−C2′−O2′] adopts gauche orientation in both N- and S-type sugar conformations.[18j]

(C) The PSEUROT Program for Analysis of Vicinal Proton−Proton *J* Couplings. The experimental $^3J_{HH}$ coupling constants were interpreted in terms of a two-state N ⇄ S pseudorotational equilibrium with the help of the computer program PSEUROT which calculates the best fit of the conformational parameters for the two-state N ⇄ S pseudorotational equilibrium to the experimental time-averaged vicinal proton−proton coupling constants.[14] The individual steps of our conformational analysis of $^3J_{HH}$ of a given interconverting pentofuranose moiety in monofluorinated nucleosides **1**−**11** are summarized in Scheme 3 (steps 1−3). The experimental $^3J_{HH}$ are time-averaged values which are linearly related to the individual coupling constants of the rapidly interconverting N and S conformers in the NMR time scale. The generalized Karplus−Altona equation[11] relates (step 1 in Scheme 3) $^3J_{HH}$ coupling constants between vicinal protons to the corresponding proton−proton torsion angles (Φ_{HH}). The Φ_{HH} are related to the corresponding endocyclic torsion angles (step 2 in Scheme 3), which in turn are related to the pseudorotation parameters P and Ψ_m. The relationship between the five endocyclic torsion angles (ν_0 [C4′−O4′−C1′−C2′], ν_1 [O4′−C1′−C2′−C3′], ν_2 [C1′−C2′−C3′−C4′], ν_3 [C2′−C3′−C4′−O4′], and ν_4 [C3′−C4′−O4′−C1′]) and the phase angle of pseudorotation (P) and a maximum puckering amplitude (Ψ_m) can be described by a simple cosine function: $\nu_j = \Psi_m \cos[P + 4\pi(j - 2)/5]$. The experimental $^3J_{HH}$ are compared to the $^3J_{HH}$ calculated by PSEUROT (steps 1−3 in Scheme 3) using the values of P and Ψ_m of both N- and S-type conformers as well as their respective populations defined in the user's input. In the following iterative steps the random changes are made in P and Ψ_m values as well as in the populations depending on the users' input, which defines the parameters to be optimized or kept fixed. The discrepancy between experimental and calculated $^3J_{HH}$ is monitored and optimized. When the best fit is found, the optimized geometries of the N and S conformers, and their populations are printed out together with the error analysis which shows both individual differences between experimental and calculated $^3J_{HH}$ as well as the overall rms error.

Clearly, an unambiguous assessment of the vicinal proton−fluorine coupling constants from fluorinated nucleoside derivatives would lead to their conformational analysis in solution. The necessary prerequisite is the availability of a Karplus-type relationship between the vicinal proton−fluorine coupling constants and proton−fluorine torsion angles (step 8 in Scheme 3). In the five-membered furanose ring both proton−proton and proton−fluorine torsion angles are related to the endocyclic torsion angles (steps 2 and 9 in Scheme 3) which can be expressed as a function of the parameters P and Ψ_m (see above) by taking the laws of pseudorotation (steps 3 and 10 in Scheme 3) into consideration. Since Altona[11] et al. have already quantitatively correlated the relationship between $^3J_{HH}$ coupling constants and the vicinal protons to the corresponding proton−proton torsion angles (Φ_{HH}), it was clear at the outset that the use of $^3J_{HF}$ in combination with $^3J_{HH}$ would greatly increase the number of known experimental values which will in principle better define the unknown pseudorotational parameters and the respective populations of the pseudorotamers.

(D) Pseudorotational Analysis for Monofluorinated Nucleosides (Steps 1−5 in Scheme 3). (i) What is the effect of fluorine substitution in the pentose sugar in 1−11? The conformations of furanose rings in **1**−**11** were analyzed on the basis of temperature-dependent (in 5 or 10 deg steps from 268 K to 363 K) vicinal proton−proton coupling constants (see Table 1 for $^3J_{HH}$ at two extreme temperatures) via the PSEUROT[14] program. For all monofluoro nucleosides **1**−**11** a high preference for one of the puckered forms in the N ⇄ S equilibria was found (Table 2), owing to the interplay between the anomeric effect of the nucleobase and the gauche effects arising from the interaction of various electronegative substituents in the sugar ring. The strong electronegativity of the fluorine atom at either C2′ or C3′ makes the C−F bond adopt a preferential gauche orientation with the ring oxygen (i.e., $C_{4'}-O_{4'}$ or C1′−O4′ bond) in **1**−**11**,[3−6] and this gauche effect is the predominant factor that governs the overall sugar conformation. Owing to the favorable gauche orientation of C4′−O4′ and C3′−F3′/F3″ bonds, the 3′−F on the β-face drives the N ⇄ S equilibium in 2′,3′-dideoxypentofuranosyl moiety to N-type,[13] whereas 3″-F on the α-face drives the sugar to S-type conformation (compare data for **11** and **4** in Table 2, respectively). When fluorine is bound to C2′, there is additionally another gauche interaction between C2′−F2′/F2″ and C1′−N bonds. The comparison of the conformational preferences in **9** (F2′ on β-face) and **10** (F2″ on α-face) shows that in the former both [O4′−C1′−C2′−F2′] and [N1−C1′−C2′−F2′] fragments adopt energeticaly preferred gauche conformation, whereas in the latter [O4′−C1′−C2′−F2″] gauche effect seems to predominate over the weaker gauche effect of [N1−C1′−C2′−F2″] fragments.[13,18i]

(19) (a) Feigon, J.; Wang, A. H.-J.; van der Marel, G. A.; van Boom, J. H.; Rich, A. *Nucleic Acids Res.* **1984**, *12*, 1243. (b) Tran-Dinh, S.; Taboury, J.; Neumann, J.-M.; Huynh-Dinh, T.; Genissel, B.; Laglois d'Estaintot, B.; Igolen, J. *Biochemistry* **1984**, *23*, 1362. (c) Davis, P. W.; Hall, K.; Cruz, P.; Tinoco, I.; Neilson, T. *Nucleic Acids Res.* **1986**, *14*, 1279. (d) Davis, P. W.; Adamiak, R. W.; Tinoco, I. *Biopolymers* **1990**, *29*, 109. (e) Agback, P.; Sandstrom, A.; Yamakage, S.-I.; Sund, C.; Glemarec, C.; Chattopadhyaya, J. *J. Biochem. Biophys. Methods* **1993**, *27*, 229. (f) Agback, P.; Glemarec, C.; Yin, L.; Sandstrom, A.; Plavec, J.; Sund, C.; Yamakage, S.-I.; Wiswanadham, G.; Rousse, B.; Puri, N.; Chattopadhyaya, J. *Tetrahedron Lett.* **1993**, *34*, 3929.

Table 1. The Experimental $^3J_{HH}$ and $^3J_{HF}$ Coupling Constants at the Two Extreme[a] Temperatures

	T	$J_{1'2'}$	$J_{1'2''}$	$J_{2'3'}$	$J_{2'3''}$	$J_{2''3'}$	$J_{2''3''}$	$J_{3'4'}$	$J_{3''4'}$	$J_{1'F2'}$	$J_{1'F2''}$	$J_{2'F}$	$J_{2''F}$	$J_{3'F}$	$J_{3'F''}$	$J_{3''F}$	$J_{4'F}$
FLT (**1**)	278	9.3	5.6	5.2		1.4		1.3				38.6	21.7				27.6
	358	8.8	5.9	5.6		1.7		1.8				36.5	22.9				27.2
FLT5 (**2**)	273	9.5	5.2	4.9		0.8		1.6				39.9	20.1				28.6
	313	9.4	5.3	5.1		1.0		1.6				38.8	20.3				28.2
AFLT (**3**)	278	8.8	6.0	5.1		2.0		1.8				34.6	22.8				26.8
	318	8.7	6.0	5.6		2.0		1.9				33.3	23.1				26.6
F3″ddU (**4**)	283	9.1	5.7	5.1		0.7		1.0				38.7	21.2				27.2
	353	8.7	5.9	5.5		1.3		1.6				36.8	24.0				27.2
FXA (**5**)	298	2.0			1.6				3.3			14.3					28.8
	363	2.6			1.8				3.6			15.7					28.4
FXA5 (**6**)	268	0.9			1.3				2.8			13.8					30.7
	313	2.3			1.8				3.3			16.4					27.6
FXA25 (**7**)	273	1.5			0.6				2.8			13.0					30.5
	303	1.6			1.0				2.6			13.3					30.3
F3AT (**8**)	273		3.4			1.1		2.1					15.1				27.7
	303		3.6			1.5		2.5					15.3				27.2
F2'ddU (**9**)	283		3.2			1.6	5.5	5.0	8.7	18.8				27.9		36.3	
	353		3.4			2.4	5.8	5.6	8.3	18.0				28.9		33.9	
F2″ddU (**10**)	283	0.9		4.5	0.5			11.5	4.7		18.1				42.8	20.3	
	353	0.9		5.0	0.9			10.9	5.2		18.9				41.2	21.2	
F3'ddU (**11**)	283	2.0	8.2		0.3		4.5		2.4			23.4	43.2				30.4
	353	2.4	8.1		0.6		4.7		2.8			24.3	42.2				30.4
F3'ddA (**24**)	298	1.7	8.0		0.7		4.5		2.7			21.6	42.6				29.9
	353	2.3	8.0		0.9		4.5		2.8			22.8	41.8				29.9
F2″C (**25**)	298	1.4		4.7				9.0			19.7				22.5		
	353	1.5		4.8				8.5			19.7				21.2		
diFA (**26**)	298							8.0		5.8	10.1			10.2	12.6		
	353							7.5		6.7	9.9			9.5	12.9		
diFG (**27**)	298							8.1		5.5	10.7			10.8	12.2		
	353							7.8		6.3	10.4			10.1	12.8		
diFT (**28**)	298							8.5		8.2	8.2			11.9	11.9		
	353							8.0		6.6	10.0			10.8	12.8		
diFC (**29**)	298							8.3		6.3	9.1			11.7	11.7		
	353							8.0		6.1	9.5			10.1	13.1		

[a] Vicinal coupling constants (in Hertz, ±0.1 Hz) are only given at two extreme temperatures (in K). They are, however, available at intermediate temperatures and were used in the conformational analysis: FLT (**1**) [from 278 to 358 K in 5 deg steps], FLT5 (**2**) [293 K], AFLT (**3**) [298 K], FXA (**5**) [323 and 343 K], FXA5 (**6**) [283 and 295 K], FXA25 (**7**) [288 K], F3AT (**8**) [288 K], F3″ddU (**4**), F2′ddU (**9**), F2″ddU (**10**), and F3′ddU (**11**) [300, 313, and 333 K, see ref 13], and F3′ddA (**24**), F2″C (**25**), diFA (**26**), diFG (**27**), diFT (**28**), and diFC (**29**) [313 and 333 K].

Table 2. Geometries of the Major Pseudorotamers and Their Respective Populations at Two Extreme Temperatures for 1−11, 24, and 25 Obtained from PSEUROT (Version 5.4) Analyses[a] of Temperature-Dependent $^3J_{HH}$ Coupling Constants

	P_N	$\Psi_m{}^N$	P_S	$\Psi_m{}^S$	$x_S{}^{lowT}$	$x_S{}^{highT}$	rms	ΔJ^{max}
FLT (**1**)	−20.0[b]	30.0[b]	143.3	33.7	0.92	0.86	0.2	0.3
FLT5 (**2**)	−18.0[b]	34.5[b]	140.9	34.8	0.93	0.92	0.4	0.6
AFLT (**3**)	0.2[b]	32.0[b]	151.9	32.0	0.85	0.84	0.1	0.3
F3″ddU (**4**)	−30.0[b]	30.0[b]	146.8	31.6	0.95	0.88	0.4	0.6
FXA (**5**)	30.0	32.1	145.0[b]	33.0[b]	0.13	0.20	<0.1	0.1
FXA5 (**6**)	26.1	33.3	140.0[b]	33.0[b]	0.00	0.17	0.1	0.5
FXA25 (**7**)	39.9	33.6	160.0[b]	33.0[b]	0.00	0.01	0.1	0.5
F3AT (**8**)	18.2[b]	35.0[b]	135.8	35.5	0.94	0.88	0.1	0.1
F2′ddU (**9**)	−32.4	40.0[b]	131.1	40.0[b]	0.89	0.79	0.2	0.3
F2″ddU[c] (**10**)	19.0	34.0	160.0[b]	40.0[b]	0.00	0.00	0.2	0.6
F3′ddU (**11**)	29.9	33.7	180.0[b]	40.0[b]	0.00	0.00	0.3	0.6
F3′ddA (**24**)	23.0	33.0	140.0[b]	41.0[b]	0.00	0.00	0.2	0.3
F2″C (**25**)	45.3	37.2	180.0[b]	40.0[b]	0.00	0.05	0.1	0.1

[a] Pseudorotational parameters are given in degrees, root-mean-square error (rms), and the maximum deviations between experimental and calculated coupling constants (ΔJ^{max}) are in Hz. The PSEUROT program version 5.4[14] has been used. [b] This parameter was kept fixed during the least-squares optimization. [c] See ref 13.

(ii) The Construction of $^3J_{HF}$ versus Φ_{HF} dataset for a New Proton−Fluorine Karplus−Type Equation. The pseudorotational analyses with PSEUROT[14] program (steps 1−3 in Scheme 3) of monofluorinated nucleosides **1**−**11** based on $^3J_{HH}$ gave a set of P and Ψ_m values characterizing the major conformers. These were used to calculate the proton−fluorine torsion angles (step 4 in Scheme 3) with the use of the following relation: $\Phi_{HF} = A_F\nu j + B_F$, where $j = 0-4$. A_F and B_F parameters were obtained from a series of ab initio calculations at the HF/3-21G level with the GAUSSIAN 94 program[20] on **1**, **3**−**5**, and **8**−**11** (see the Experimental Section). From the geometries of **1**, **3**−**5**, and **8**−**11** optimized by ab initio, the sets of Φ_{HF} and the corresponding endocyclic torsion angles were extracted and used to parametrize linear relations $\Phi_{HF} = A_F\nu_j + B_F$. The resulting ($A_F$ and B_F) parameter sets for each of the H−F pairs are given in Table 3.

The fact that a particular $^3J_{HF}$ in each of the monofluorinated nucleosides **1**−**11** varies linearly while the equilibrium populations of the N and S conformers change with temperature enabled us to extrapolate the observed $^3J_{HF}$ coupling constants to the "limiting" coupling constants in the major conformer (step 5 in Scheme 3). Note that in the pseudorotational concept the geometry (i.e., P and Ψ_m) of the individual conformers participating in the equilibrium does not change with temperature. The limiting $^3J_{HF}$ values found for the major conformers and the respective Φ_{HF} torsion angles

(20) Frisch, M. J.; Trucks, G. W.; Schlegel, H. B.; Gill, P. M. W.; Johnson, B. G.; Robb, M. A.; Cheeseman, J. R.; Keith, T.; Petersson, G. A.; Montgomery, J. A.; Raghavachari, K.; Al-Laham, M. A.; Zakrzewski, V. G.; Ortiz, J. V.; Foresman, J. B.; Cioslowski, J.; Stefanov, B. B.; Nanayakkara, A.; Challacombe, M.; Peng, C. Y.; Ayala, P. Y.; Chen, W.; Wong, M. W.; Andres, J. L.; Replogle, E. S.; Gomperts, R.; Martin, R. L.; Fox, D. J.; Binkley, J. S.; Defrees, D. J.; Baker, J.; Stewart, J. P.; Head-Gordon, M.; Gonzalez, C.; Pople, J. A. *Gaussian 94*, Revision C.3; Gaussian, Inc.: Pittsburgh, PA, 1995.

Table 3. *A* and *B* Parameters[a] for the Correlation of Endocyclic C−C Torsions with H−H Torsions and H−F Torsions from Constrained Sugar Geometries Optimized Using GAUSSIAN Program at HF/3-21G Level

	FLT (**1**) and FLT5 (**2**)		AFLT (**3**)		F3″ddU (**4**)		FXA (**5**) and **6**−**7**		F3AT (**8**)		F2′ddU (**9**)		F2″ddU (**10**)		F3′ddU (**11**)		diFA (**26**) and **27**−**29**	
	A (*σ*)	*B* (*σ*)	*A* (*σ*)	*B* (*σ*)	*A* (*σ*)	*B* (*σ*)	*A* (*σ*)	*B* (*σ*)	*A* (*σ*)	*B* (*σ*)	*A* (*σ*)	*B* (*σ*)	*A* (*σ*)	*B* (*σ*)	*A* (*σ*)	*B* (*σ*)	*A* (*σ*)	*B* (*σ*)
$\Phi_{1'2'}$	1.11 (0.03)	119.8 (0.8)	1.12 (0.02)	119.5 (0.7)	1.08 (0.06)	119.2 (1.3)	1.09 (0.02)	120.0 (0.6)					1.07 (0.07)	116.1 (1.6)	1.03 (0.08)	122.4 (2.0)		
$\Phi_{1'2''}$	1.07 (0.02)	−2.6 (0.6)	1.12 (0.02)	−2.1 (0.5)	1.05 (0.05)	−3.0 (1.2)			1.11 (0.02)	−1.0 (0.4)	0.99 (0.04)	2.5 (0.9)			1.02 (0.08)	0.6 (1.9)		
$\Phi_{2'3'}$	1.17 (0.01)	−2.5 (0.2)	1.12 (0.01)	−2.6 (0.2)	1.17 (0.01)	−2.5 (0.2)							1.20 (0.02)	4.0 (0.4)				
$\Phi_{2'3''}$							1.14 (0.01)	−117.7 (0.3)					1.17 (0.02)	−117.8 0.5	1.14 (0.04)	−119.5 (1.0)		
$\Phi_{2''3'}$	1.15 (0.01)	119.9 (0.2)	1.15 (0.01)	119.7 (0.2)	1.16 (0.00)	119.3 (0.1)			1.18 (0.01)	119.4 (0.2)	1.12 (0.01)	121.9 (0.2)						
$\Phi_{2''3''}$											1.12 (0.01)	0.2 (0.3)		(0.04)	1.14 (1.0)	2.2		
$\Phi_{3'4'}$	1.04 (0.02)	−120.0 (0.7)	1.06 (0.01)	−121.1 (0.5)	0.99 (0.04)	−120.3 (1.1)			1.13 (0.02)	−121.8 (0.6)	1.03 (0.04)	−127.0 (1.0)	1.04 (0.05)	−124.1 (1.4)			1.08 (0.04)	−123.9 (1.1)
$\Phi_{3''4'}$							1.06 (0.01)	−4.3 (0.4)			1.03 (0.04)	−4.1 (1.0)	1.05 (0.05)	−0.9 (1.3)	0.99 (0.06)	−6.6 (1.5)		
$\Phi_{H1'F2'}$											0.97 (0.04)	122.2 (1.0)					1.07 (0.05)	116.1 (1.3)
$\Phi_{H1'F2''}$													1.05 (0.06)	−3.8 (1.5)			1.07 (0.05)	−3.0 (1.2)
$\Phi_{H2'F}$	1.15 (0.01)	−124.8 (0.2)	1.17 (0.01)	−123.8 (0.3)	1.14 (0.01)	−124.4 (0.3)	1.15 (0.03)	2.8 (0.4)							1.14 (0.03)	0.3 (0.7)		
$\Phi_{H2''F}$	1.13 (0.01)	−2.3 (0.2)	1.15 (0.01)	−1.5 (0.3)	1.12 (0.00)	−2.6 (0.1)			1.18 (0.01)	−0.7 (0.2)					1.14 (0.03)	122.0 (0.8)		
$\Phi_{H3'F2'}$											1.13 (0.4)	0.4 (0.4)					1.20 (0.03)	3.4 (0.8)
$\Phi_{H3'F2''}$													1.19 (0.02)	126.4 (0.4)			1.21 (0.02)	122.9 (0.7)
$\Phi_{3''F}$											1.12 (0.02)	−121.2 (0.4)	1.17 (0.02)	4.3 (0.5)				
$\Phi_{4'F}$	1.05 (0.02)	−0.1 (0.7)	1.07 (0.02)	−1.2 (0.48)	1.00 (0.04)	−1.12 (1.1)	1.04 (0.01)	−125.4 (0.4)	1.13 (0.02)	−0.7 (0.6)					1.02 (0.06)	−125.5 (1.6)		

[a] See the Experimental Section for the details of the ab initio calculations.

are presented in Table 4. The perusal of the $^3J_{HF} - \Phi_{HF}$ data set in Table 4 shows that proton−fluorine torsion angles are not distributed over the complete torsion angle range; most of the Φ_{HF} values are found in the cis ($-34° < \Phi_{HF} < 42°$) and in the trans regions ($155° < \Phi_{HF} < 165°$ and $200° < \Phi_{HF} < 206°$) only. With the use of data from the conformationally fixed compounds **12**−**17** (step 6 in Scheme 3), Φ_{HF} torsion angles around 90° were introduced, which were not available from the conformational analysis of nucleosides **1**−**11**. For monofluoronucleosides in our dataset (i.e., entries 1−29 in Table 4), only three trans couplings ($^3J_{2'F3''}$) larger than 43 Hz [i.e., 43.5 Hz for FLT (**1**) (entry 1), 44.5 Hz for FLT5 (**2**) (entry 4), and 45.3 Hz for AFLT (**3**) (entry 7)] were available from the extrapolated temperature-dependent coupling constant analysis, hence experimentally determined limiting trans coupling constants for the conformationally frozen systems were introduced. Berthelot[22] and Lankin[21] showed that these limiting $^3J_{HF}$ values may be ≈45−47 Hz for some trans substitution patterns in fluorinated Decalins **22** and **23**[22] (entry 57−59 in Table 4) and fluoro piperidines[21] **18**−**21** (entries 43−56 in Table 4), which were introduced in our dataset to increase the confidence level of our parametrization of the Karplus equation in the trans region. The $^3J_{HF} - \Phi_{HF}$ data from the conformationally constrained compounds **16** and **17** also allowed us to take into consideration geminal difluoro substitution (entries 40−42 in Table 4).

It is noteworthy that for all conformationally constrained compounds **12**−**22**, the Φ_{HF} torsion angle values presented in Table 4 correspond to the values extracted from their ab initio optimized geometries (at HF/3-21G level) (see the Experimental Section).

The use of the limiting $^3J_{HF}$ and the corresponding Φ_{HF} torsion angles from pseudorotational analysis of monofluorinated nucleosides **1**−**11** in combination with the literature data on **12**−**22** resulted in 57 data points (Table 4) which were the basis for the formulation and evaluation (step 7 in Scheme 3) of our new Karplus-type equation for $^3J_{HF}$.

(E) Parametrization of a Karplus-Type Equation for $^3J_{HF}$ Coupling Constants. (i) The Inadequacy of a Simple Three-Term Karplus Equation (Eq 1). The examination of our data set of 57 $^3J_{HF}$ coupling constants and the respective proton−fluorine torsion angles (Table 4) shows that all regions of Φ_{HF} torsion angles are indeed covered. The comparison of data for $J_{H2''F3''}$ in F3AT (**8**) and $J_{H3'F2'}$ in F2′ddU (**9**) (entries 19 and 22 in Table 4, respectively) shows that although they are characterized with nearly identical proton−fluorine torsion angles in the cis range (−30°) their limiting $^3J_{HF}$ coupling constants are 14.9 and 26.8 Hz, respectively. It is interesting to note that variation in $^3J_{HF}$ coupling constants in the trans region of Φ_{HF} ranges is up to about 16 Hz, which is evident from the comparison of entries 7 and 14 in Table 4 ($J_{H2'F3''} = 45.3$ Hz in AFLT (**3**) and $J_{H4'F3'} = 29.5$ Hz in FXA (**5**), respectively). It is therefore clear that a simple three-parameter Karplus equation cannot adequately correlate our 57 $^3J_{HF} - \Phi_{HF}$ calibration points.

(21) Lankin, D. C.; Chandrakumar, N. S.; Rao, S. N.; Spangler, D. P.; Snyder, J. P. *J. Am. Chem. Soc.* **1993**, *115*, 3356.
(22) Berthelot, J.-P.; Jacquesy, J.-C.; Levisalles, J. *Bull. Soc. Chim. Fr.* **1971**, *5*, 1896.

Table 4. Limiting $^3J_{HF}$, the Corresponding H−C−C−F Torsion Angles, Substituent Electronegativities, Bond Angles from the Major Pseudorotamers of 1−11 and Conformationally Fixed Compounds 12−22 in Comparison with the Calculated $^3J_{HF}$ using Karplus-Type Equation (1)[a,b]

			input experimental data								results from Karplus eq	
entry	compound[c]	$^3J_{HF}$	J_{exp}	Φ_{HF}	λ_1	λ_2	λ_3	λ_4	a_{FCC}	a_{HCC}	J_{calc}	$J_{calc}-J_{exp}$[b]
1	FLT (**1**)	$J_{2'F3''}$	43.5	204.5	0.6	0.0	0.6	0.0	109.2	107.4	41.4	2.1
2	FLT (**1**)	$J_{2''F3''}$	19.6	327.5	0.0	0.6	0.6	0.0	109.2	113.2	21.0	−1.4
3	FLT (**1**)	$J_{4'F3''}$	28.5	10.6	1.3	0.7	0.0	0.7	107.0	109.4	29.3	−0.8
4	FLT5 (**2**)	$J_{2'F3''}$	44.5	204.1	0.6	0.0	0.6	0.0	109.2	107.4	41.6	2.9
5	FLT5 (**2**)	$J_{2''F3''}$	19.3	327.1	0.0	0.6	0.6	0.0	109.2	113.2	20.9	−1.6
6	FLT5 (**2**)	$J_{4'F3''}$	30.1	9.3	1.3	0.7	0.0	0.7	107.0	109.4	29.5	0.6
7	AFLT (**3**)	$J_{2'F3''}$	45.3	203.2	0.6	0.0	0.6	0.0	108.6	107.8	42.4	2.9
8	AFLT (**3**)	$J_{2''F3''}$	19.4	326.0	0.0	0.6	0.6	0.0	108.6	113.9	20.3	−0.9
9	AFLT (**3**)	$J_{4'F3''}$	29.0	13.7	1.3	0.7	0.0	0.7	106.4	109.6	29.4	−0.4
10	F3″ddU (**4**)	$J_{2'F3''}$	39.9	205.6	0.6	0.0	0.6	0.0	109.8	107.6	39.6	0.3
11	F3″ddU (**4**)	$J_{2''F3''}$	20.3	327.7	0.0	0.6	0.6	0.0	109.8	112.9	20.7	−0.5
12	F3″ddU (**4**)	$J_{4'F3''}$	27.2	10.1	1.3	0.7	0.0	0.7	107.8	109.7	27.4	−0.2
13	FXA (**5**)	$J_{2'F3'}$	11.9	34.9	0.6	1.3	0.0	0.6	107.9	114.2	11.9	−0.0
14	FXA (**5**)	$J_{4'F3'}$	29.5	201.4	1.3	0.7	0.6	0.0	108.2	110.9	31.1	−1.6
15	FXA5 (**6**)	$J_{2'F3'}$	13.7	37.3	0.6	1.3	0.0	0.6	107.9	114.2	11.1	2.6
16	FXA5 (**6**)	$J_{4'F3'}$	30.7	200.5	1.3	0.7	0.6	0.0	108.2	110.9	31.4	−0.7
17	FXA25 (**7**)	$J_{2'F3'}$	13.1	32.5	0.6	1.3	0.0	0.6	107.9	114.2	12.8	0.3
18	FXA25 (**7**)	$J_{4'F3'}$	30.5	199.8	1.3	0.7	0.6	0.0	108.2	110.9	31.6	−1.1
19	F3AT (**8**)	$J_{2''F3''}$	14.9	329.3	1.3	0.6	0.6	0.0	109.2	113.3	12.8	2.1
20	F3AT (**8**)	$J_{4'F3''}$	28.2	6.2	1.3	0.7	0.0	0.6	108.7	110.1	25.8	2.4
21	F2′ddU (**9**)	$J_{1'F2'}$	19.7	159.9	0.6	1.3	0.0	0.7	112.8	113.6	20.0	−0.3
22	F2′ddU (**9**)	$J_{3'F2'}$	26.8	330.9	0.0	0.6	0.6	0.0	108.9	109.9	27.5	−0.7
23	F2′ddU (**9**)	$J_{3''F2'}$	39.1	209.3	0.6	0.0	0.6	0.0	108.9	108.1	38.1	1.0
24	F2″ddU (**10**)	$J_{1'F2''}$	18.5	335.8	0.6	1.3	0.7	0.0	109.0	111.2	20.4	−1.9
25	F2″ddU (**10**)	$J_{3'F2''}$	42.0	164.7	0.0	0.6	0.0	0.6	106.6	111.0	43.7	−1.7
26	F2″ddU (**10**)	$J_{3''F2''}$	20.7	41.8	0.6	0.0	0.0	0.6	106.6	111.2	21.7	−1.0
27	F3′ddU (**11**)	$J_{2'F3'}$	23.7	33.5	0.6	0.0	0.0	0.6	108.3	111.4	24.1	−0.4
28	F3′ddU (**11**)	$J_{2''F3'}$	42.7	155.3	0.0	0.6	0.0	0.6	108.3	107.7	42.2	0.5
29	F3′ddU (**11**)	$J_{4'F3'}$	30.4	200.3	1.3	0.7	0.7	0.0	109.6	109.5	31.1	−0.7
30	**12**	J_{AF}	30.8	12.6	0.6	0.6	0.6	0.6	107.2	107.1	32.1	−1.3
31	**12**	J_{BF}	3.8	288.8	0.6	0.6	0.6	0.6	107.4	110.7	3.9	−0.1
32	**13**	J_{AF}	19.8	6.5	0.6	0.6	0.6	0.6	113.4	108.3	19.7	0.1
33	**13**	J_{BF}	2.0	78.8	0.6	1.3	0.6	0.6	111.2	114.7	0.2	1.8
34	**15**	J_{HAFA}	13.1	357.8	0.9	0.0	1.4	0.9	111.5	113.1	11.1	2.0
35	**15**	J_{HAFB}	7.4	236.2	0.9	0.0	0.9	1.4	109.4	113.1	8.7	−1.3
36	**15**	J_{HBFA}	4.5	120.1	0.0	0.9	1.4	0.9	111.5	112.1	6.9	−2.4
37	**15**	J_{HBFB}	15.9	358.4	0.0	0.9	0.9	1.4	109.4	112.1	17.2	−1.3
38	**14**	J_{HAFA}	13.9	357.8	1.4	0.9	0.9	0.0	113.3	110.9	11.8	2.0
39	**14**	J_{HBFB}	17.7	358.4	1.4	0.9	0.9	0.0	110.7	109.2	19.9	−2.2
40	**16**	J_{HAFA}	9.1	357.8	1.4	0.9	0.9	1.4	111.8	109.9	7.1	2.1
41	**16**	J_{HAFB}	0.3	120.0	1.4	0.9	1.4	0.9	110.2	109.9	2.4	−2.1
42	**17**	J_{H4F2}	2.1	77.5	0.6	0.6	1.4	0.6	114.5	113.4	1.0	1.1
43	**18**	J_{H2axF}	38.7	170.8	0.8	0.0	0.8	0.0	105.7	113.5	39.3	−0.6
44	**18**	J_{H4axF}	44.5	184.7	0.0	0.8	0.0	0.7	105.8	112.1	43.4	1.1
45	**18**	J_{H2eqF}	9.7	296.5	0.0	0.8	0.8	0.0	105.7	109.2	10.0	−0.3
46	**18**	J_{H4eqF}	9.3	66.5	0.8	0.0	0.0	0.7	105.8	106.5	9.5	−0.2
47	**19**	J_{H2axF}	34.3	172.2	0.8	0.0	0.8	0.4	104.9	114.6	36.2	−1.9
48	**19**	J_{H4axF}	44.4	182.9	0.0	0.8	0.4	0.7	104.7	111.3	44.3	0.1
49	**19**	J_{H2eqF}	10.2	296.7	0.0	0.8	0.8	0.4	104.9	109.6	9.4	0.8
50	**19**	J_{H4eqF}	10.6	64.6	0.8	0.0	0.4	0.7	104.7	107.5	9.8	0.8
51	**20**	J_{H4axF}	44.4	177.4	0.0	0.6	0.0	0.7	108.2	110.7	43.1	1.3
52	**20**	J_{H6axF}	37.5	178.9	0.8	0.0	0.8	0.0	107.5	112.8	38.5	−1.0
53	**21**	J_{H2axF}	34.3	186.0	1.0	0.0	0.8	0.4	109.6	110.3	35.0	−0.7
54	**21**	J_{H4axF}	44.4	178.0	0.0	0.8	0.4	0.7	107.5	108.7	44.0	0.4
55	**21**	J_{H2eqF}	10.2	302.3	0.0	1.0	0.8	0.4	109.6	107.1	10.8	−0.6
56	**21**	J_{H4eqF}	10.6	61.5	0.8	0.0	0.4	0.7	107.5	105.3	11.3	−0.7
57	**22**	J_{HaxF}	46.0	171.3	0.8	0.5	0.0	0.5	106.7	108.2	46.5	−0.5
58	**23**	J_{HBF}	47.0	187.2	0.5	0.0	0.5	0.8	107.7	107.9	45.5	−1.5
59	**23**	J_{HAF}	47.0	181.8	0.0	0.8	0.5	0.5	104.1	110.1	48.7	1.7

[a] $^3J_{HF}$ coupling constants are in Hz and Φ_{HF} torsion angles and a_{FCC} and a_{HCC} bond angles are in degrees. $\lambda_1-\lambda_4$ are the empirical group electronegativities[14] of the α-substituents at positions 1−4. [b] Rms deviation between input and back-calculated $^3J_{HF}$ values using eq 3 is 1.4 Hz. [c] The $^3J_{HF}$ data have been taken from ref 13 for F2′ddU (**9**), F2″ddU (**10**), F3′ddU (**11**), and F3″ddU (**4**), ref 10a for **12** and **13**, ref 10b for **14**−**16**, ref 10f for **17**, ref 21 for **18**−**21**, and ref 22 for **22** and **23**.

The inspection of H−C−C−F coupling pathways in nucleosides **1**−**11** and in **12**−**22** shows that the large variability of $^3J_{HF}$ at the particular Φ_{HF} torsion angle range can be correlated with their *substitution patterns* (compare substituent λ electronegativities in Table 4). These considerations have led us to set up a six-parameter Karplus equation (A−F in eq 1), which includes terms of the generalized Haasnoot−Altona equation[11] used in the analysis of $^3J_{HH}$.

$$^3J_{HH} = A\cos^2\Phi + B\cos\Phi + C + \Sigma\lambda_i[D + E\cos^2(\xi_i\Phi + F\lambda_i)] \quad (1)$$

The optimum values for the six parameters $A-F$ were determined by Monte Carlo minimization using Profit

program[23] with 57 $^3J_{HF}$ values, torsion angles, and the corresponding substituent λ electronegativities of α-substituents on vicinal carbon atoms (Table 4). The fit was not satisfactory which was evident from the large discrepancy of up to 10 Hz between the input and back-calculated $^3J_{HF}$ values for some calibration points. The poor quality of the fit has stimulated our search for additional terms, which have indeed improved correlation of $^3J_{HF}$ and Φ_{HF} (Table 4).

(ii) The Introduction of the Bond-Angle Term to Give a Seven-Parameter Karplus Equation 2. The assessment of several trial equations[24] has led us to formulate generalized Karplus-type eq 2 in which *bond angle* changes along H−C−C−F coupling pathway are correlated with a cosine-square of Φ_{HF} torsion angle.[11,12]

$$^3J_{HF} = A\cos^2\Phi + B\cos\Phi + C + \sum\lambda_i[D + E\cos^2(\xi_i\Phi + F\lambda_i)] + G[(a_{FCC} + a_{HCC})/2 - 110]\cos^2\Phi \quad (2)$$

In eq 2, Φ is a H−C−C−F torsion angle, λ_i represents the substituent electronegativity of all four substituents attached to H−C−C−F fragment, ξ_i accounts for the orientation of the α substituent and has a value of +1 or −1 depending on the orientation of the substituent, and a_{FCC} and a_{HCC} are bond angles in the H−C−C−F fragment. The first three terms (characterized by parameters *A*, *B*, and *C*) in eq 2 describe the torsion angle dependence of $^3J_{HF}$, while the next three parameters (i.e., *D*, *E*, and *F*) describe its dependence on the electronegativity of substituents and their relative orientation. The last term (characterized by parameter *G*) in eq 2 describes dependence of $^3J_{HF}$ on the F−C−C and H−C−C bond angle changes.

(iii) The Best-Iterated A−G Parameter Set for Equation 2 To Give Equation 3. The optimum values of seven parameters in eq 2 were determined by the Monte Carlo minimization[23] using 57 $^3J_{HF}$ values, Φ_{HF} torsion angles, corresponding four substituent λ electronegativities, and two bond angles (Table 4) and resulted in the Karplus-type eq 3.

$$^3J_{HF} = 40.61\cos^2\Phi - 4.22\cos\Phi + 5.88 + \sum\lambda_i[-1.27 - 6.20\cos^2(\xi_i\Phi + 0.20\lambda_i)] - 3.72[(a_{FCC} + a_{HCC})/2 - 110]\cos^2\Phi \quad (3)$$

The least-squares fit is satisfactory which is evident from the fact that all input $^3J_{HF}$ values are reproduced within Δ*J* below 2.9 Hz with rms deviation of 1.38 Hz between input and back-calculated $^3J_{HF}$ values (Table 4).

In particular, we found, consistent with Altona's observation, that the iterated *A* and *C* values are interrelated.[14e] Our basis for the choice of the above *A*−*G* parameter set is that it gives both low rms values as well as minimal negative $^3J_{HF}$ coupling constants (all $^3J_{HF} \geq -0.5$ Hz) for torsions around 90° and 270° for the substitution patterns in our dataset. Other correlated combinations of *A*−*G* parameters were excluded in view of the above selection criteria.

The individual discrepancy of 2.9 Hz (entries 4 and 7 in Table 4) requires some discussion in view of the inherent error of generalized Karplus eq 1 for $^3J_{HH}$ coupling constants which originally showed overall rms values of 0.48 Hz which dropped to 0.36 Hz with the use of the λ electronegativity scale. First, there are possibly other terms, such as the change in bond distance or complex correlation of the individual terms in eq 3, that could improve the fit between experimental and back-calculated $^3J_{HF}$ values. Second, the rms error of 1.4 Hz for Karplus eq 3 represents an error of about 4% for transoid $^3J_{HF}$ coupling constant on the order of about 40−46 Hz. This 4% error in the experimental and back-calculated $^3J_{HF}$ is reasonably acceptable in view of about 5% error encountered in the experimental and back-calculated $^3J_{HH}$ (an rms error of 0.4 Hz) for a typical transoid $^3J_{HH}$ of 8−9 Hz in Karplus−Altona's eq 1. Clearly, the availability of other fluorinated compounds which will cover more cisoidal versus transoidal couplings with well-defined geometries will certainly improve the quality of the parametrization.

(iv) The Assessment of Equation 3 Through a Simple Plot of $^3J_{HF}$ versus Φ_{HF} and Phase Angle. Figure 1 shows how $^3J_{HF}$ coupling constants vary with the change of Φ_{HF} torsion angles for a particular stereochemical position of fluorine in a nucleoside. The positions of our $^3J_{HF} - \Phi_{HF}$ calibration points close to the calculated curves in Figure 1 show that the agreement between input and back-calculated $^3J_{HF}$ is indeed satisfactory. Plots of $^3J_{HF}$ coupling constants in Figure 1 also show that there is a common difference of 5−10 Hz betwen cis and trans coupling for all the substitution patterns. The minima of the calculated curves are found in the expected regions of around ± 90°.

The plots of $^3J_{HF}$ as a function of phase angle of pseudorotation in Figure 2 for various configurations at C2′ or C3′ in fluorinated nucleosides show a qualitative way to assess the conformational bias of the sugar ring and a relatively simple way to estimate the predominance of N- or S-type pseudorotamers in solution from the experimental $^3J_{HF}$ coupling constants. The plots in Figure 2 also offer the possibility to qualitatively differentiate between the C3′-*endo*, C3′-*endo*-C2′-*exo*, and C2′-*exo* puckered sugar geometry in the N region, and between the C3′-*exo*, C3′-*exo*-C2′-*endo*, and C2′-*endo* puckered sugar geometry in the S region of conformational space from the relative position of individual experimental $^3J_{HF}$ coupling constants. In the case of FLT (**1**), for example, $J_{H2''F3''}$ coupling constant shows a maximum at *P* around 180° (see panel A in Figure 2). At the same *P*, $J_{H2''F3''}$ coupling constant in FLT (**1**) is at minimum, whereas $J_{H4'F3''}$ is not and has a minimum at $P = 220°$.

(v) The Qualitative Assessment of Validity of Equation 3 on Compounds 1−11 Using Plots of $^3J_{HF}$ vs $^3J_{HH}$. Our best-fit Karplus-type eq 3 for $^3J_{HF}$ coupling constants has been evaluated on a set of monofluorinated

(23) PROFIT II 4.1, Quantum Soft, Postfach 6613, CH-8023 Zürich, Switzerland, 1990.

(24) We initially tried to use different formalisms and data sets in order to correlate $^3J_{HF}$ coupling constants with the corresponding H−C−C−F torsion angles, in the following manner: (i) a simple reparametrization of the Haasnoot−Altona equation (eq 1 in the text) using λ substituent electronegativities on 57 data points resulted in an rms larger than 4 Hz and individual differences of ≈12 Hz for F2′ddU (**9**) ($^3J_{H1'F2'}$) and ≈8 Hz for William1 ($^3J_{HAF}$); (ii) to investigate the influence of the electronegativity scales, we have also tried to reparametrize eq 1 on the basis of a limited dataset [for instance, 19 J_{HF}/Φ_{HF} pairs from nucleosides only, including the data for FLT (**1**), FLT (**5**), FXA (**5**), FXA5 (**6**), FXA25 (**7**), F3AT (**8**), AFT (**3**), and F2″C (**25**)] using Huggins electronegativities instead of λ substituent parameters, which was however not successful ($\chi^2 \approx 235$, individual differences of ≈5−7 Hz).

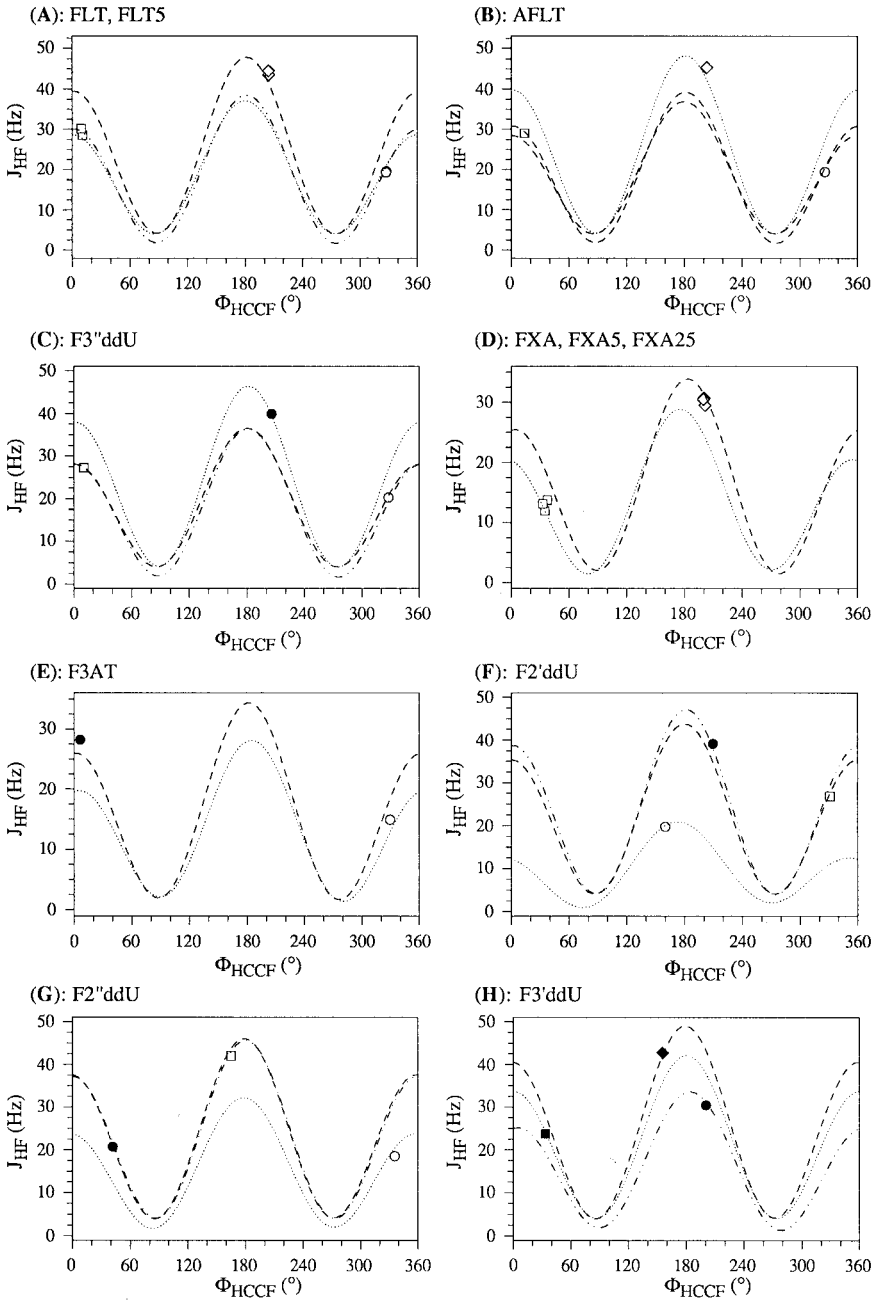

Figure 1. The plots of vicinal $^3J_{HF}$ versus $\Phi_{H-C-C-F}$ torsion angles for **1**−**11**. The plots have been made using our Karplus equation with the best-fit *A*−*G* parameter set in eq 3. Substituent electronegativities for each H−C−C−F fragment as well as the F−C−C and H−C−C bond angles are shown in columns 6−9 for λ_1−λ_4 and columns 10 and 11, respectively, in Table 4. The experimental data for both J_{HF} and Φ_{HF} are shown in Table 4 (columns 4 and 5). (**A**) The plots of $^3J_{H2'F3''}$ versus $\Phi_{H2'-C2'-C3'-F3''}$ (•••), $^3J_{H2''F3''}$ versus $\Phi_{H2''-C2'-C3'-F3''}$ (---), and $^3J_{H4'F3''}$ versus $\Phi_{H4'-C4'-C3'-F3''}$ (−••) for FLT (**1**) and FLT5 (**2**). The pairs of limiting ($^3J_{HF}$, $\Phi_{H-C-C-F}$) of the major pseudorotamer for **1** and **2** are shown with ◇ (for $^3J_{H2'F3''}$), ○ (for $^3J_{H2''F3''}$), and □ (for $^3J_{H4'F3''}$) labels. (**B**) The plots of $^3J_{H2'F3''}$ versus $\Phi_{H2'-C2'-C3'-F3''}$ (•••), $^3J_{H2''F3''}$ versus $\Phi_{H2''-C2'-C3'-F3''}$ (---), and $^3J_{H4'F3''}$ versus $\Phi_{H4'-C4'-C3'-F3''}$ (−••) for AFLT (**3**). The pairs of limiting ($^3J_{HF}$, $\Phi_{H-C-C-F}$) of the major pseudorotamer for **3** are shown with ◇ ($^3J_{H2'F3''}$), ○ ($^3J_{H2''F3''}$), and □ ($^3J_{H4'F3''}$) labels. (**C**) The plots of $^3J_{H2'F3''}$ versus $\Phi_{H2'-C2'-C3'-F3''}$ (•••), $^3J_{H2''F3''}$ versus $\Phi_{H2''-C2'-C3'-F3''}$ (---) and $^3J_{H4'F3''}$ versus $\Phi_{H4'-C4'-C3'-F3''}$ (−••) for F3″ddU (**4**). The pairs of limiting ($^3J_{HF}$, $\Phi_{H-C-C-F}$) of the major pseudorotamer for **4** are shown with ● ($^3J_{H2'F3''}$), ○ ($^3J_{H2''F3''}$), and □ ($^3J_{H4'F3''}$) labels. (**D**) The plots of $^3J_{H2'F3'}$ versus $\Phi_{H2'-C2'-C3'-F3'}$ (•••) and $^3J_{H4'F3'}$ versus $\Phi_{H4'-C4'-C3'-F3'}$ (---) for FXA (**5**), FXA5 (**6**), and FXA25 (**7**). The pairs of limiting ($^3J_{HF}$, $\Phi_{H-C-C-F}$) of the major pseudorotamer for **5**−**7** are shown with □ ($^3J_{H2'F3'}$) and ◇ ($^3J_{H4'F3'}$) labels. (**E**) The plots of $^3J_{H2''F3''}$ versus $\Phi_{H2''-C2'-C3'-F3''}$ (•••) and $^3J_{H4'F3''}$ versus $\Phi_{H4'-C4'-C3'-F3''}$ (---) for F3AT (**8**). The pairs of limiting ($^3J_{HF}$, $\Phi_{H-C-C-F}$) of the major pseudorotamer for **8** are shown with ○ ($^3J_{H2''F3''}$) and ● ($^3J_{H4'F3''}$) labels. (**F**) The plots of $^3J_{H1'F2'}$ versus $\Phi_{H1'-C1'-C2'-F2'}$ (•••), $^3J_{H3'F2'}$ versus $\Phi_{H3'-C3'-C2'-F2'}$ (---), and $^3J_{H3''F2'}$ versus $\Phi_{H3''-C3'-C2'-F2'}$ (−••) for F2′ddU (**9**). The pairs of limiting ($^3J_{HF}$, $\Phi_{H-C-C-F}$) of the major pseudorotamer for **9** are shown with ○ ($^3J_{H1'F2'}$), □ ($^3J_{H3'F2'}$), and ● ($^3J_{H3''F2'}$) labels. (**G**) The plots of $^3J_{H1'F2''}$ versus $\Phi_{H1'-C1'-C2'-F2''}$ (•••), $^3J_{H3'F2''}$ versus $\Phi_{H3'-C3'-C2'-F2''}$ (---), and $^3J_{H3''F2''}$ versus $\Phi_{H3''-C3'-C2'-F2''}$ (−••) for F2″ddU (**10**). The pairs of limiting ($^3J_{HF}$, $\Phi_{H-C-C-F}$) of the major pseudorotamer for **10** are shown with ○ ($^3J_{H1'F2''}$), □ ($^3J_{H3'F2''}$), and ● ($^3J_{H3''F2''}$) labels. (**H**) The plots of $^3J_{H2'F3'}$ versus $\Phi_{H2'-C2'-C3'-F3'}$ (•••), $^3J_{H2''F3'}$ versus $\Phi_{H2''-C2'-C3'-F3'}$ (---), and $^3J_{H4'F3'}$ versus $\Phi_{H4'-C4'-C3'-F3'}$ (−••) for F3′ddU (**11**). The pairs of limiting ($^3J_{HF}$, $\Phi_{H-C-C-F}$) of the major pseudorotamer for **11** are shown with ■ ($^3J_{H2'F3'}$), ◆ ($^3J_{H2''F3'}$), and ● ($^3J_{H4'F3'}$) labels.

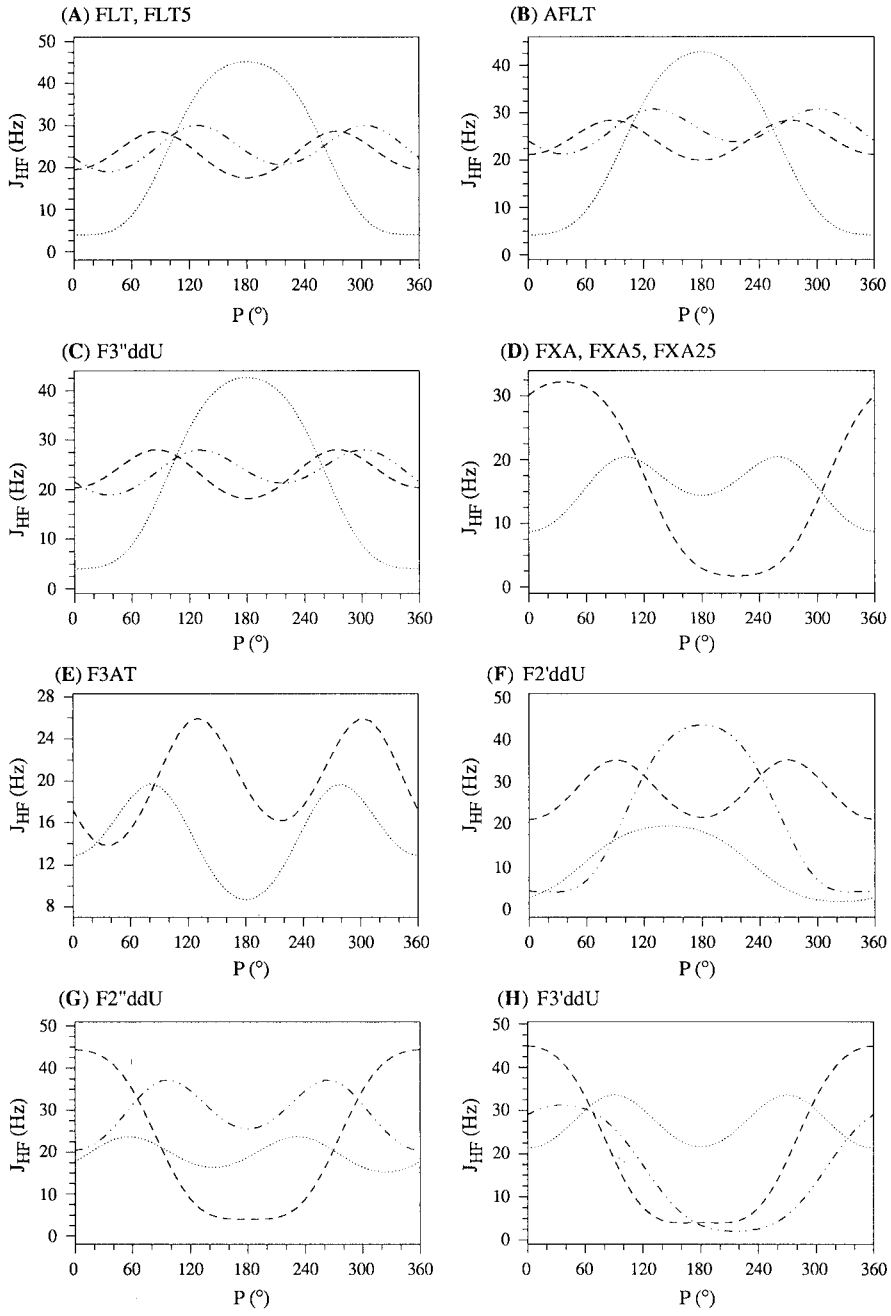

Figure 2. (A) The plots of $^3J_{H2'F3''}$ (•••), $^3J_{H2''F3''}$ (---), and $^3J_{H4'F3''}$ (-•••) for FLT (**1**) and FLT5 (**2**) have been made at $\Psi_m = 34°$. (**B**) The plots of $^3J_{H2'F3''}$ (•••), $^3J_{H2''F3''}$ (---), and $^3J_{H4'F3''}$ (-•••) for AFLT (**3**) at $\Psi_m = 29°$. (**C**) The plots of $^3J_{H2'F3''}$ (•••), $^3J_{H2''F3''}$ (---), and $^3J_{H4'F3''}$ (-•••) for F3″ddU (**4**) with $\Psi_m = 32°$. (**D**) The plots of $^3J_{H2'F3'}$ (•••) and $^3J_{H4'F3'}$ (---), for FXA (**5**), FXA5 (**6**), and FXA25 (**7**) at $\Psi_m = 36°$. (**E**) The plots of $^3J_{H2''F3''}$ (•••) and $^3J_{H4'F3''}$ (---) for F3AT (**8**) at $\Psi_m = 36°$. (**F**) The plots of $^3J_{H1'F2'}$ (•••), $^3J_{H3'F2'}$ (---), and $^3J_{H3''F2''}$ (-•••) for F2″ddU (**9**) at $\Psi_m = 36°$. (**G**) The plots of $^3J_{H1'F2''}$ (•••), $^3J_{H3'F2''}$ (---), and $^3J_{H3''F2''}$ (-•••) for F2″ddU (**10**) at $\Psi_m = 34°$. (**H**) The plots of $^3J_{H2'F3'}$ (•••), $^3J_{H2''F3'}$ (---), and $^3J_{H4'F3'}$ (-•••) for F3′ddU (**11**) at $\Psi_m = 34°$.

nucleosides **1**−**11** (Scheme 1). In the first exploratory step, we have constructed plots of $^3J_{HF}$ and $^3J_{HH}$ coupling constants as a function of *P* at various Ψ_m for **1**−**11** (Figures 3−5). This graphical analysis of conformational preferences in **1**−**11** has clearly shown in a qualitative way that the use of $^3J_{HF}$ and $^3J_{HH}$ coupling constants gives comparable results. The position of both experimental $^3J_{HF}$ and $^3J_{HH}$ in FLT (**1**) and FLT5 (**2**) relative to the calculated curves of $^3J_{HF}$ versus $^3J_{HH}$ coupling constants as a function of *P*, which is systematically varied from 0° via 180° to 360° in 10° steps at $\Psi_m = 34°$, shows that the sugar conformation is biased toward S (ca. 85%) with P around 160° [see panels A−D in Figure 3]. In the case of AFLT (**3**), the N ⇄ S equilibrium is shifted toward S which is evident from the position of experimental $^3J_{2'F}$ and $^3J_{4'F}$ versus $^3J_{1'2'}$ and $^3J_{3'4'}$ in panels E−G in Figure 3. The position and alignment of experimental $^3J_{HF}$ and $^3J_{HH}$ in F3″ddU (**4**) relative to the calculated curves in panels I−J in Figure 3 show that its sugar conformation is biased toward S (ca. 90%). The experimental $^3J_{HF}$ and $^3J_{HH}$ data points for FXA (**5**) and FXA5 (**6**) in panels K−L of Figure 3 show a great preference for N-type sugar conformation. In the case of F3AT (**8**) there is a great preference for S-type sugar conformation [panels A−B in Figure 4]. The experimental $^3J_{HF}$ and $^3J_{HH}$ in F2′ddU (**9**) are positioned close to

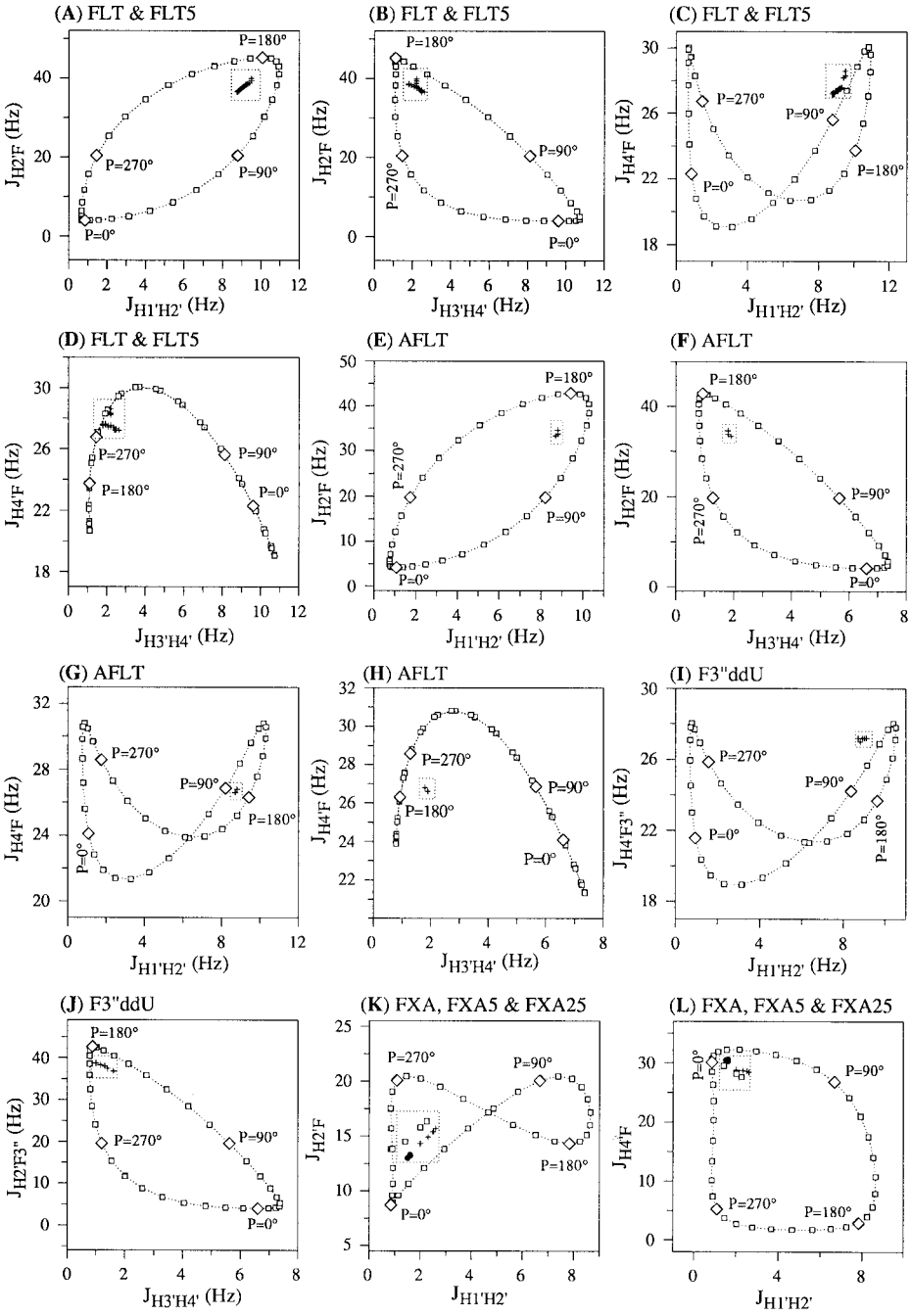

Figure 3. The plots showing the theoretical change of $^3J_{HF}$ versus $^3J_{HH}$ at a particular value of Ψ_m over the whole pseudorotation cycle for monofluoronucleosides **1**−**7**, and in the dotted square box in each panel, the experimental data points of the variation of $^3J_{HF}$ versus $^3J_{HH}$ as a function of the temperature (see Table 1 for the $^3J_{HF}$ versus $^3J_{HH}$ values at two extreme temperatures). Each theoretical plot has been made using (i) the set of A_F (or A_H) and B_F (or B_H) parameters that translate H−C−C−F (or H−C−C−H) torsions into the endocyclic torsion angles (Table 3) according to the following relation: $\Phi_{HF/HH} = A_{F/H}{*}\Psi_m \cos[P + (j - 2)2\pi/5) + B_{F/H}$, where $j = 1$, 2, or 3, depending on which endocyclic torsion is used (i.e., either ν_1, ν_2, or ν_3, step 10 and then 9 in Scheme 3); (ii) our Karplus equation with the "best" set of $A-F$ parameters (i.e., eq 3 in the text) with the $\lambda_1-\lambda_4$ substituent parameters shown in Table 4 (columns 6−9) for H−C−C−F fragments (see the Experimental Section for the substituent electronegativities in H−C−C−H fragments) and the values for the F−C−C and H−C−C bond angles compiled in columns 10 and 11 of Table 4. The value of P has been varied from 0° to 360° in 10° steps to calculate the corresponding H−C−C−F and H−C−C−H torsion angles. On each plot, we have marked the (J_{HF}, J_{HH}) coordinate pairs at $P = 0°$, $P = 90°$, $P = 180°$, and $P = 270°$ with the ◇ symbol. (A−D) The plots of the calculated variations of $J_{H2'F}$ versus $J_{H1'H2'}$ (panel A), $J_{H2'F}$ versus $J_{H3'4'}$ (panel B), $J_{H4'F}$ versus $J_{H1'H2'}$ (panel C), and $J_{H4'F}$ versus $J_{H3'H4'}$ (panel D) for FLT (**1**) and FLT5 ($\Psi_m = 34°$) (**2**). The experimental data for FLT (**1**) and FLT5 (**2**) are shown with the + sign in the box. (E−H) The plots of the calculated variations of $J_{H2'F}$ versus $J_{H1'H2'}$ (panel E), $J_{H2'F}$ versus $J_{H3'4'}$ (panel F), $J_{H4'F}$ versus $J_{H1'H2'}$ (panel G), and $J_{H4'F}$ versus $J_{H3'H4'}$ (panel H) for AFLT (**3**) ($\Psi_m = 29°$). The experimental data for AFLT (**1**) are shown with the + sign. (I and J) The plots of the calculated variations of $J_{H4'F3''}$ versus $J_{H1'H2'}$ (panel I) and $J_{H2'F3''}$ versus $J_{H3'H4'}$ (panel J) for F3″ddU (**4**) ($\Psi_m = 32°$). The experimental data are shown with the + sign. (K and L) The plots of the calculated variations of $J_{H2'F3'}$ versus $J_{H1'H2'}$ (panel K) and $J_{H4'F3'}$ versus $J_{H1'H2'}$ (panel L) for FXA (**5**) ($\Psi_m = 36°$). The experimental data are shown with the sign + for FXA (**5**), □ for FXA5 (**6**), and ● for FXA25 (**7**).

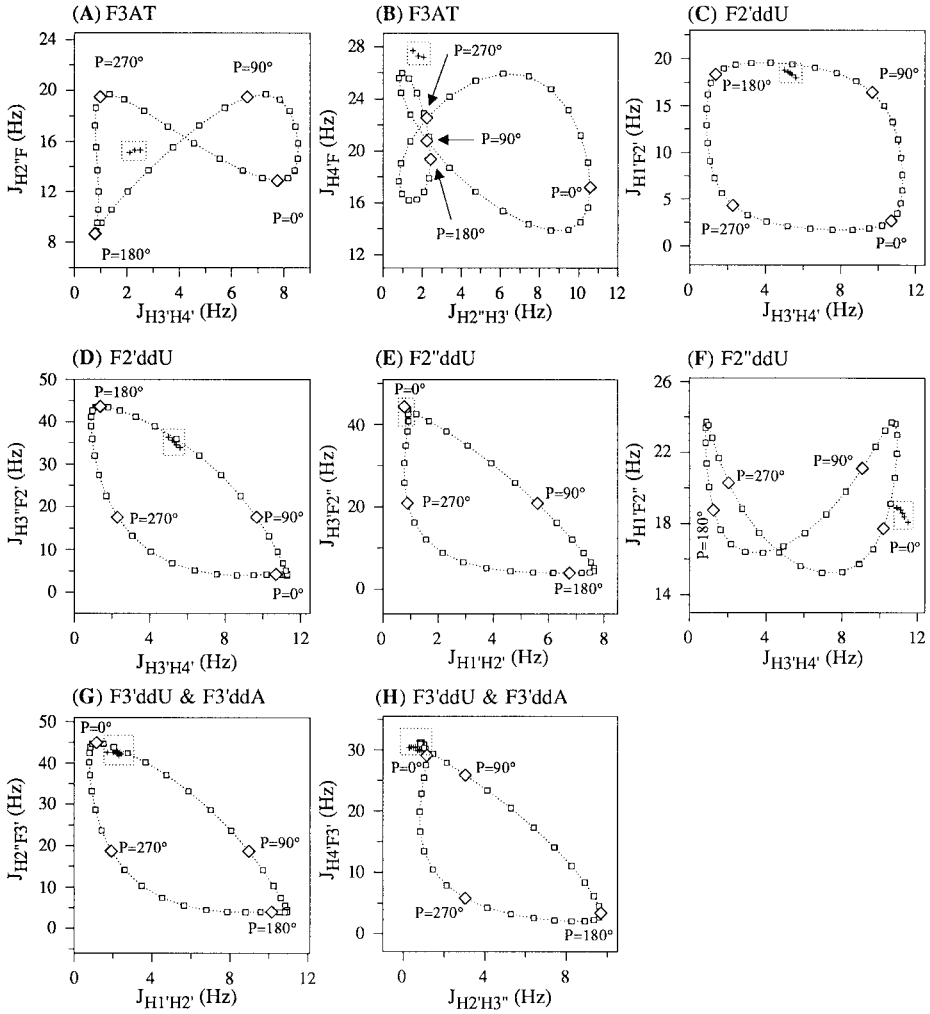

Figure 4. The plots of the theoretical change of $^3J_{HF}$ versus $^3J_{HH}$ at a particular value of Ψ_m over the whole pseudorotation cycle for monofluoronucleosides **8**−**11** and **24** and the experimental data of the variation of $^3J_{HF}$ and $^3J_{HH}$ with the temperature, marked the + symbol in the dotted box (see the legend of Figure 3 for the description of the method used to made the plots). (A and B) The plots of the calculated variations of $J_{H2''F3''}$ versus $J_{H3'H4'}$ (panel A) and $J_{H4'F3''}$ versus $J_{H2''H3'}$ (panel B) for F3AT (**8**) ($\Psi_m = 36°$). (C and D) The plots of the calculated variations of $J_{H1'F2'}$ versus $J_{H3'H4'}$ (panel C) and $J_{H3''F2'}$ versus $J_{H3'H4'}$ (panel D) for F2′ddU (**9**) ($\Psi_m = 36°$). (E and F) The plots of the calculated variations of $J_{H3'F2''}$ versus $J_{H1'H2'}$ (panel E) and $J_{H1'F2''}$ versus $J_{H3'H4'}$ (panel F) for F2″ddU (**10**) ($\Psi_m = 34°$). (G and H) The plots of the calculated variations of $J_{H2''F3'}$ versus $J_{H1'H2'}$ (panel G), $J_{H4'F3'}$ versus $J_{H2'H3''}$ (panel H) for F3′ddU (**11**) and F3′ddA (**24**) ($\Psi_m = 34°$).

the calculated curves in panels C and D in Figure 4 which indicates over 95% of S-type conformer with *P* around 140°. On the other hand, the experimental $^3J_{HF}$ and $^3J_{HH}$ in F2″ddU (**10**) [panels E and F] and F3′ddU (**11**) [panels G and H] are positioned close to the calculated curves which indicates nearly 100% population of N-type conformer with *P* between ≈−10° and 20° (Figure 4).

As such graphical analysis of the conformational preferences of fluorinated nucleosides is only qualitative, we have made a more quantitative use of our Karplus eq 3 by modifying the computer program PSEUROT to use the experimental $^3J_{HF}$ coupling constants in addition to or in combination with the $^3J_{HH}$ for the conformational analysis of fluorinated nucleosides.

(F) The New "PSEUROT+J_{HF}" Program for the Quantitative Assessment of the Validity of Equation 3. The program PSEUROT+J_{HF} (see Experimental Section for a short description of the changes made to PSEUROT to obtain the PSEUROT+J_{HF} program) is based on program PSEUROT (ver. 3B)[14] and calculates the least-squares fit of the five pseudorotational parameters defining the two-state N ⇄ S pseudorotational equilibrium to the set of experimental $^3J_{HF}$ coupling constants. The individual steps of conformational analysis of $^3J_{HF}$ of a given interconverting pentofuranose moiety in monofluorinated nucleosides are summarized in Scheme 3 (steps 8−10). The temperature-dependent experimental $^3J_{HF}$ are time-averaged, and they are linearly related to the coupling constants of the individual N and S conformers. The generalized Karplus-type eq 3 relates (step 8 in Scheme 3) $^3J_{HF}$ coupling constants between vicinal proton and fluorine atoms to the corresponding proton−fluorine torsion angles (Φ_{HF}). The Φ_{HF} are related to the corresponding endocyclic torsion angles (step 9 in Scheme 3), which in turn are related to the pseudorotation parameters *P* and Ψ_m (step 10 in Scheme 3). The PSEUROT+J_{HF} program also uses the input of $^3J_{HH}$ coupling constants alone or in combination with $^3J_{HF}$. In this case, both steps 1−3 and steps 8−10 in Scheme 3 are used in the iterative analysis to define the N ⇄ S pseudorotational equilibrium of a fluorinated nucleoside. The quality of the fit is assessed through the calculation of the rms deviation between the experimental and calculated $^3J_{HF}$ and $^3J_{HH}$ values. When the five

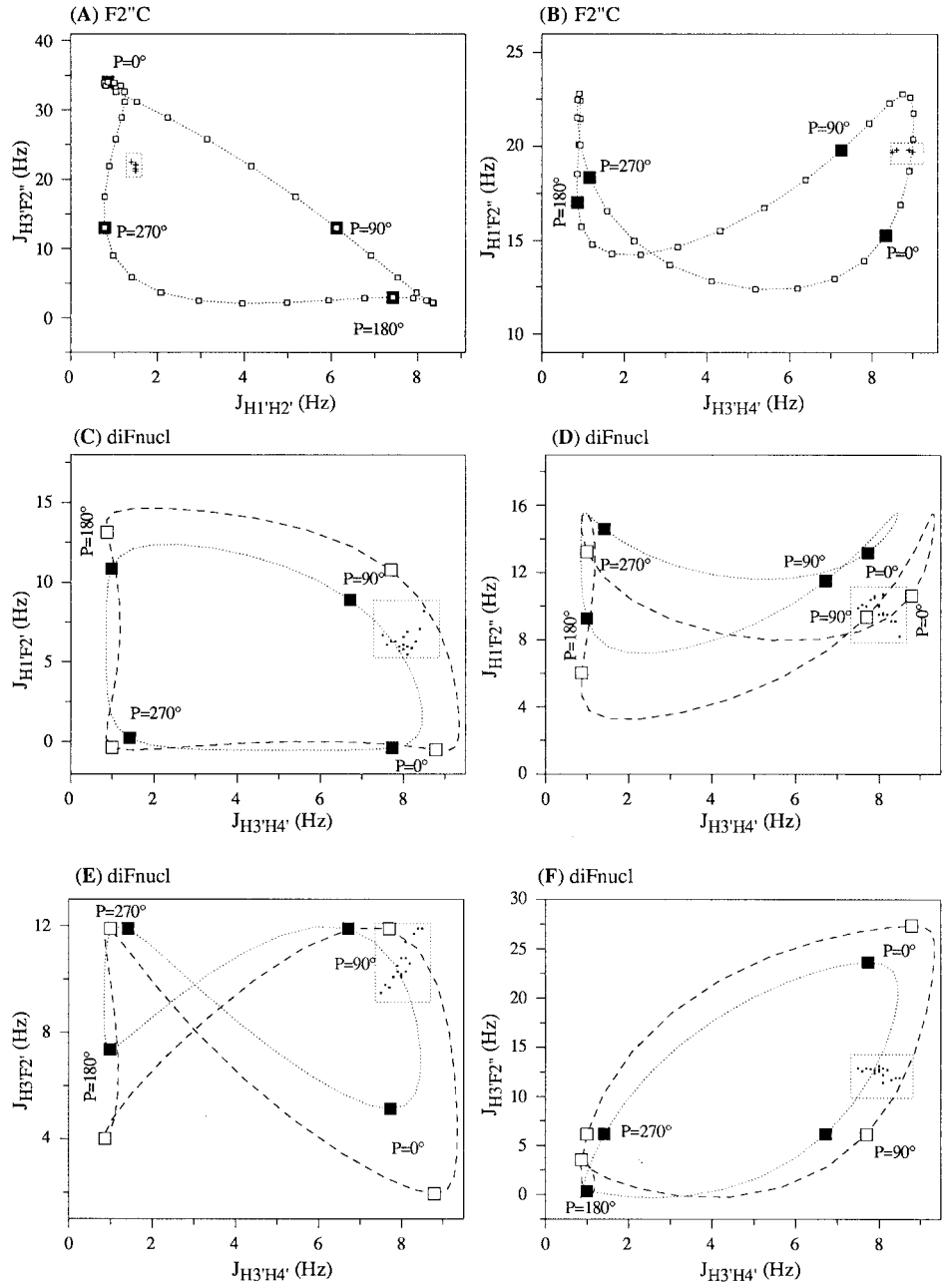

Figure 5. The plots of the theoretical change of $^3J_{HF}$ versus $^3J_{HH}$ at one or two particular values of Ψ_m over the whole pseudorotation cycle for F2″C (**25**) and for difluoronucleosides **26**−**29** and the experimental data of the variation of $^3J_{HF}$ and $^3J_{HH}$ with the temperature, marked the + or dot symbol in the dotted box (see the legend of Figure 3 for the description of the method used to made the plots). (A and B) The plots of the calculated variations of $J_{H3'F2''}$ versus $J_{H1'H2'}$ (panel A) and $J_{H1'F2''}$ versus $J_{H3'H4'}$ (panel B) for F2″C (**25**) (Ψ_m = 39°). (C and F) The plots of the calculated variations of $J_{H1'F2'}$ versus $J_{H3'H4'}$ (panel C), $J_{H1'F2''}$ versus $J_{H3'H4'}$ (panel D), $J_{H3'F2'}$ versus $J_{H3'H4'}$ (panel E), and $J_{H3'F2''}$ versus $J_{H3'H4'}$ (panel F) at Ψ_m = 33° (···) and 45° (---) for diFA (**26**), diFG (**27**), diFT (**28**), and diFC (**29**).

parameters cannot be defined by the experimental coupling constants it is necessary to keep some *P* and Ψ_m fixed during the least-squares iterative procedure, just as in the original PSEUROT program. In the case of strongly biased N ⇄ S conformational equilibrium, the pseudorotation parameters of the minor component are constrained to obtain the parameters of the more interesting major component. When both N- and S-type pseudorotamers are present in approximately equal amounts, both Ψ_m values are constrained to assume equal values. In either way, the fluctuations in the population of N- and S-type conformers at a particular temperature are observed.

(G) The Application of Karplus-Type Equation 3 and PSEUROT+J_{HF} in the Conformational Analysis of Fluorinated Nucleosides. (i) A Qualitative Assessment of Validity of Equation 3 on 24 and 25 Using Plots of $^3J_{HF}$ versus $^3J_{HH}$. The Karplus-type eq 3 for $^3J_{HF}$ coupling constants has first been applied to the conformational analysis of monofluorinated nucleosides **24** and **25** in a graphical manner. The experimental $^3J_{HF}$ and $^3J_{HH}$ in F3′ddA (**24**) are positioned close to the calculated curves which indicates nearly 100% population of N-type conformer with *P* between −10° and 20° [panels G and H, Figure 4]. The position of experimental $^3J_{HF}$ and $^3J_{HH}$ in panels A and B in Figure 5 relative to the

calculated curves shows that the sugar conformation in F2″C (**25**) is biased toward N (>95%).

(ii) An Assessment of the Validity of our Karplus Equation through the Calculation of trans Coupling Constant in Decalin Derivative 23. It may also be noted that our Karplus equation is able to predict trans $^3J_{HF}$ coupling constant (i.e., $^3J_{HBF}$ and $^3J_{HAF}$) values of Decalin derivative **23** rather close ($^3J_{calc} - {}^3J_{exp} < 1.7$ Hz, Table 4) to the experimentally measured value (47 Hz).[22,25]

(iii) A Qualitative Conformational Analysis of 26 − 29 using Plots of $^3J_{HF}$ versus $^3J_{HH}$ based on Equation 3. Our best fit Karplus-type eq 3 for $^3J_{HF}$ coupling constants has been used to construct plots of $^3J_{HF}$ versus $^3J_{H3'H4'}$ coupling constants as a function of *P* from 0° via 180° to 360° in 10° steps at Ψ_m 33° and 45° for difluorinated nucleosides **26**−**29** (Figure 5). The examination of the position and the alignment of experimental $^3J_{HF}$ and $^3J_{H3'H4'}$ in difluorinated nucleosides **26**−**29** shows that their conformations are very similar and biased toward N-type with *P* in the range from 50° to 90° [panels C−F in Figure 5]. In the case of **26**−**29** only a single proton−proton coupling constant (i.e., $^3J_{H3'H4'}$) is available, which makes it impossible to assess their solution conformation on the basis of $^3J_{HH}$ alone. The use of $^3J_{HF}$ coupling constants along with $^3J_{HH}$ enabled us to perform the conformational analysis of their sugar moieties for the first time.

(iv) The Quantitative and Comparative Analysis of Fluorinated Nucleosides Using PSEUROT+J_{HF} Program. In a more elaborate conformational analysis of **1**−**11** and **26**−**29**, we have used the computer program PSEUROT+J_{HF} which calculates the best fit of experimental $^3J_{HF}$ and $^3J_{HH}$ coupling constants to the *P* and Ψ_m for both N- and S-type conformers and corresponding mole fractions. The PSEUROT+J_{HF} program was used in three ways: (i) only $^3J_{HH}$ coupling constants, (ii) only $^3J_{HF}$ coupling constants, and (iii) temperature-dependent $^3J_{HH}$ and $^3J_{HF}$ coupling constants together. The results of these analyses are presented in Table 5.

The comparison of the data for the major pseudorotamers of **1**−**11** and **24**−**25** in Table 5 from the analysis of $^3J_{HH}$ and $^3J_{HF}$ coupling constants alone with PSEUROT+J_{HF} program shows that: (i) the largest difference in the values for *P* is 35° for AFLT (**3**), (ii) the Ψ_m values differ by up to 12−13° for FLT (**1**) and AFLT (**3**), (iii) the populations of the major conformers at the lowest temperature differ by up to 11 unit % for F2′ddU (**9**), whereas the differences in populations for other nucleosides are smaller than 8 unit %, (iv) the rms error is below 0.8 and 0.7 Hz from the analysis of $^3J_{HH}$ and $^3J_{HF}$ coupling constants alone, respectively, and (v) the largest individual discrepancy between experimental and calculated coupling constants is 1.2 Hz for $^3J_{HH}$ and 2.0 Hz for $^3J_{HF}$.

The conformational analysis of **1**−**11** and **24**−**25** has also been performed via two additional sets of PSEUROT+J_{HF} calculations, both of these sets being based on experimental $^3J_{HH}$ as well as $^3J_{HF}$ coupling constants (see also footnote *d* of Table 5). In the first set of calculations [see right-hand side of Table 5, first line of P − x_S (high) parameters for each compound], the individual errors between experimental and back-calculated coupling constants produced by the iterative procedure with PSEUROT+J_{HF} have been treated uniformly for calculated $^3J_{HF}$ and $^3J_{HH}$ data. In the second set of calculations (for the results, see Table 5, columns 14−20, on the second line for each compound), we have introduced a scale factor (0.2 for $^3J_{HF}$, 1.0 for $^3J_{HH}$ couplings) of the errors determined by the program between experimentally measured and back-calculated $^3J_{HF}$ and $^3J_{HH}$ coupling constants in order to account for the fact that on average the former are ≈5 times larger than the latter (i.e., ≈9 and ≈45 Hz, respectively, for torsion angles in the trans region). For details of the modifications of the original PSEUROT program, readers are directed to our web site.

A perusal of the data presented in Table 5 shows the following. (i) The analyses based on $^3J_{HH}$ as well as $^3J_{HF}$ with different scale factors for both types of coupling constants, as expected, result in smaller errors (ΔJ_{HH}, column 15) between experimentally measured and back-calculated proton−proton coupling constants than those where no scale factors have been introduced. However the overall rms of the calculations was found to be slightly higher in the former type of analyses than in the latter (compare first and second lines of rms values in column 14). The introduction of scale factors of the errors did not affect the overall sugar geometry in comparison with the analyses based on $^3J_{HH}$ and $^3J_{HF}$ data but performed in the absence of the scale factor. (ii) The values for *P* for the major pseudorotamers are as expected very similar to the values found from the conformational analysis of $^3J_{HH}$ and $^3J_{HF}$ coupling constants alone; the difference of 20° in *P* for FLT (**1**), for example, is due to the small shift in the puckering from C2′-*endo* to more C2′-*endo*-C3′-*exo* conformation. (iii) The differences in Ψ_m are on the order of few degrees and the largest difference is 9° in the case of FXA (**5**). (iv) The rms error is below 1.2 Hz (without scale factors of the errors) which is comparable to analyses when only $^3J_{HH}$ or $^3J_{HF}$ was used. (v) The largest individual discrepancy between experimental and calculated coupling constants is 2.2 Hz for $^3J_{HH}$ and 2.7 Hz for $^3J_{HF}$ (without scale factors). (vi) The populations of the major conformers at the lowest temperature differ by 9 unit % for F2′ddU (**9**), whereas the differences in populations for other nucleosides are smaller than 7% units.

The use of both experimental $^3J_{HH}$ and $^3J_{HF}$ coupling constants in the conformational analysis of **26**−**29** with the PSEUROT+J_{HF} program shows that their conformational equilibria are greatly biased toward N-type conformation (x_N (low *T*) = 78−94% at 298 K, Table 5). The geometry of the major pseudorotamers of **26**−**29** is characterized with *P* in the range from 61° to 76° which is between C4′-*exo* and O4′-*endo*-C4′-*exo* puckering. The Ψ_m values are in the range from 35° to 46° (Table 5). The analyses are characterized with rms error between 1.4 and 1.7 Hz with the maximum individual error of 1.3 Hz for $^3J_{H3'H4'}$ and 3.3 Hz for $^3J_{HF}$.

(25) Note that compound **23** has not been used during the parametrization of our Karplus equation because only one value for the trans proton−fluorine coupling constant (47 Hz) was available in the original paper (ref 22), although two coupling pathways exist. However, taking into consideration the two possible coupling pathways (see Table 4, electronegativities of the substituents in entries 58 and 59), we have been able to confirm the validity of our Karplus equation by calculating the $^3J_{HAF}$ and $^3J_{HBF}$ values using the electronegativity and bond angle values given in Table 4. Our estimates differ from the original experimental value by less than 1.7 Hz.

Table 5. The Geometry of the Major Pseudorotamer[a] of the N ⇄ S Equilibrium in 1−11 and 24−29 as Determined with the PSEUROT+J_{HF} Program Basing upon Experimental $^3J_{HH}$ and/or $^3J_{HF}$ Coupling Constants

	analyses using $^3J_{HH}$ data only[b]						analyses using $^3J_{HF}$ data only[c]						analyses using both $^3J_{HH}$ and $^3J_{HF\ data}$[d]						
compound	P (deg)	Ψ_m (deg)	rms (Hz)	ΔJ_{max} (Hz)	x_S (lowT)	x_S (highT)	P (deg)	Ψ_m (deg)	rms (Hz)	ΔJ_{max} (Hz)	x_S (lowT)	x_S (highT)	P (deg)	Ψ_m (deg)	rms (Hz)	ΔJ_{HH} (Hz)	ΔJ_{HF} (Hz)	x_S (lowT)	x_S (highT)
FLT (**1**)	150 ± 1	36 ± 2	<0.6	−0.9	0.89	0.83	171 ± 4	24 ± 1	≤0.3	−0.8	0.97	0.92	151 ± 5	29 ± 1	≤0.9	−2.0	1.7	0.94	0.88
													146 ± 2	34 ± 1	≤1.0	−1.3	2.6	0.91	0.85
FLT5 (**2**)	146 ± 1	39 ± 1	<0.8	−1.1	0.92	0.90	146 ± 6	34 ± 2	≤0.1	0.2	0.93	0.90	143 ± 3	36 ± 1	≤0.7	−1.2	−0.6	0.92	0.90
													143 ± 2	38 ± 1	≤0.8	−1.2	1.0	0.91	0.89
AFLT (**3**)	159 ± 1	35 ± 1	≤0.5	−0.6	0.84	0.82	194 ± 9	22 ± 1	≤0.1	0.3	0.90	0.86	156 ± 11	27 ± 2	≤1.2	−1.9	−1.9	0.86	0.82
													148 ± 3	32 ± 2	≤1.4	−1.3	2.6	0.83	0.81
F3″ddU (**4**)	153 ± 1	35 ± 1	≤0.8	−1.2	0.93	0.87	156 ± 1	25 ± 1	≤0.7	2.0	1.00	0.98	145 ± 1	30 ± 1	≤1.0	−1.8	2.7	1.00	0.94
													146 ± 1	33 ± 1	≤1.0	−1.5	3.7	0.96	0.90
FXA (**5**)	31 ± 2	35 ± 1	≤0.1	0.1	0.07	0.13							43 ± 2	29 ± 1	≤0.6	−0.9	0.9	0.04	0.07
													40 ± 2	30 ± 1	≤0.7	−0.7	1.7	0.04	0.09
FXA5 (**6**)	27 ± 1	36 ± 1	≤0.2	−0.5	0.00	0.10							38 ± 2	27 ± 1	≤1.0	−1.5	2.0	0.00	0.09
													33 ± 3	28 ± 1	≤1.0	−1.3	2.8	0.00	0.09
FXA25 (**7**)	35 ± 1	35 ± 1	≤0.4	−0.5	0.00	0.00							32 ± 1	30 ± 1	≤0.6	−1.4	0.3	0.00	0.00
													32 ± 1	30 ± 1	≤0.6	−1.4	0.3	0.00	0.00
F3AT (**8**)	139 ± 1	38 ± 1	≤0.1	0.1	0.98	0.91							127 ± 1	33 ± 1	≤0.9	1.0	1.8	1.00	1.00
													130 ± 1	34 ± 1	≤1.0	0.9	1.7	1.00	1.00
F2′ddU (**9**)	139 ± 1	43 ± 2	≤0.5	−1.0	0.88	0.79	135 ± 2	33 ± 1	≤0.3	−0.8	0.99	0.92	133 ± 1	37 ± 1	≤0.8	1.6	1.3	0.97	0.90
													133 ± 2	40 ± 1	≤0.9	1.5	2.8	0.92	0.86
F2″ddU (**10**)	37 ± 1	38 ± 1	≤0.4	−0.7	0.00	0.00	7 ± 2	34 ± 1	≤0.3	−0.5	0.04	0.08	15 ± 1	36 ± 1	≤0.9	−1.7	−1.5	0.03	0.07
													26 ± 1	38 ± 1	≤1.1	−0.9	−3.0	0.00	0.05
F3′ddU (**11**)	15 ± 1	36 ± 1	≤0.6	−1.0	0.00	0.02	21 ± 1	31 ± 1	≤0.3	0.7	0.00	0.00	20 ± 1	32 ± 1	≤0.7	−1.5	0.9	0.00	0.00
													18 ± 1	33 ± 1	≤0.8	−1.2	1.8	0.00	0.00
F3′ddA (**24**)	11 ± 1	37 ± 1	≤0.6	−0.8	0.00	0.03	20 ± 1	34 ± 1	≤0.3	0.7	0.04	0.06	17 ± 2	34 ± 1	≤0.7	−1.3	0.8	0.03	0.05
													13 ± 1	34 ± 1	≤0.7	−1.1	1.3	0.03	0.05
F2″C (**25**)	36 ± 1	37 ± 1	≤0.1	0.1	0.00	0.04							36 ± 3	33 ± 4	≤1.3	2.2	−0.9	0.22	0.27
													36 ± 3	33 ± 3	≤1.7	1.7	−3.2	0.16	0.20
diFA (**26**)							62 ± 4	38 ± 4	≤1.6	−3.0	0.20	0.26	66 ± 4	40 ± 6	≤1.4	1.1	−2.9	0.19	0.21
													68 ± 2	43 ± 3	≤1.4	0.4	−2.9	0.13	0.18
diFG (**27**)							61 ± 9	35 ± 5	≤1.6	−2.9	0.17	0.17	68 ± 3	37 ± 3	≤1.4	1.0	−2.9	0.14	0.14
													70 ± 2	40 ± 2	≤1.4	0.3	−2.9	0.08	0.10
diFT (**28**)							76 ± 2	46 ± 2	≤1.7	−3.4	0.08	0.01	76 ± 2	46 ± 1	≤1.5	−0.8	−3.3	0.06	0.02
													76 ± 2	46 ± 1	≤1.5	−0.8	−3.3	0.06	0.02
diFC (**29**)							68 ± 6	38 ± 4	≤2.0	−3.4	0.22	0.16	70 ± 3	40 ± 3	≤1.7	1.3	−3.2	0.14	0.09
													72 ± 2	42 ± 2	≤1.7	0.5	−3.3	0.09	0.09

[a] For each compound, the N ⇄ S pseudorotational equilibrium is heavily biased toward either N or S form. Therefore, all pseudorotational analyses[14] have been performed by constraining simultaneously P and Ψ_m of the minor pseudorotamer in the range $-30° < P_N < 30°$ in 20° steps (for the N-type conformer) or alternatively $140° < P_S < 180°$ in 20° steps (for the S-type sugar) with Ψ_m fixed at 3 or 4 values in the range 32°−41°. x_S (low T) and x_S (high T) represent the mole fraction of the South conformer at the lowest and highest experimental temperature, respectively (see Table 1). x_S (low T) and x_S (high T) have been calculated by averaging the results from all successful pseudorotational analyses. [b] The PSEUROT+J_{HF} analyses based exclusively on $^3J_{HH}$ data have been performed with 5 temperature-dependent coupling constants for **1**−**4** (i.e., $^3J_{1'2'}$, $^3J_{1'2''}$, $^3J_{2'3'}$, $^3J_{2''3'}$, and $^3J_{3'4'}$), **9** (i.e., $^3J_{1'2''}$, $^3J_{2''3'}$, $^3J_{2''3''}$, $^3J_{3'4'}$, and $^3J_{3''4'}$), **10** (i.e., $^3J_{1'2'}$, $^3J_{2'3'}$, $^3J_{2'3''}$, $^3J_{3'4'}$, and $^3J_{3''4'}$), and for **11** and **24** (i.e., $^3J_{1'2'}$, $^3J_{1'2''}$, $^3J_{2'3''}$, $^3J_{2''3''}$ and $^3J_{3''4'}$) or with 3 temperature-dependent coupling constants for **5**−**7** (i.e., $^3J_{1'2'}$, $^3J_{2'3''}$, and $^3J_{3''4'}$), **8** (i.e., $^3J_{1'2''}$, $^3J_{2''3'}$, and $^3J_{3'4'}$), and **25** (i.e., $^3J_{1'2'}$, $^3J_{2'3'}$, and $^3J_{3'4'}$) (see the Experimental Section). [c] These PSEUROT+J_{HF} analyses are based on 3 or 4 temperature-dependent $^3J_{HF}$ data, that is, $^3J_{F3''H2'}$, $^3J_{F3''H2''}$ and $^3J_{F3''H4'}$ for **1**−**4**, $^3J_{F2'H1'}$, $^3J_{F2'H3'}$, and $^3J_{F2'H3''}$ for **9**, $^3J_{F2''H1'}$, $^3J_{F2''H3'}$, and $^3J_{F2''H3''}$ for **10**, $^3J_{F3'H2'}$, $^3J_{F3'H2''}$, and $^3J_{F3'H4'}$ for **11** and **24**, and $^3J_{F2'H1'}$, $^3J_{F2''H1'}$, $^3J_{F2'H3'}$, and $^3J_{F2''H3'}$ for **26**−**29**. [d] The PSEUROT+J_{HF} analyses based on all experimentally available $^3J_{HH}$ and $^3J_{HF}$ coupling constants have been performed in two ways: (i, first line of parameter values in columns 14−20): either by treating equally the errors (i.e., J_{diff}, where $J_{diff} = J_{exp} - J_{calc}$) calculated between experimental (J_{exp}) and back-calculated (J_{calc}) $^3J_{HH}$ and $^3J_{HF}$ during the iteration process with PSEUROT (note that this is the default case in a PSEUROT calculation) or (ii) by using different scale factors (sf) for J_{diff} values relative to proton−proton (sf = 1.0) and proton−fluorine (sf = 0.2) coupling constants during the minimization procedure. The purpose of the analyses performed according to (ii) was to take into consideration the fact that $^3J_{HH}$ couplings are on average ≈5 times smaller than the corresponding $^3J_{HF}$ for the same value of the torsion angle Φ_{HH} or Φ_{HF}. Therefore, attributing the same weighting factors to $^3J_{HH}$ and $^3J_{HF}$ data resulted in rather high ΔJ_{HH} errors (column 17) in the analyses performed according to (i) in comparison with the errors (column 5) of the PSEUROT analyses based exclusively on $^3J_{HH}$ couplings. Five temperature-dependent $^3J_{HH}$ (see footnote *a*) and 3 $^3J_{HF}$ (see footnote *b*) have been used for **1**−**4**, **9**−**11**, and **18**; 3 $^3J_{HH}$ (see footnote *a*) and 2 $^3J_{HF}$ (i.e., $^3J_{F3'H2'}$ and $^3J_{F3'H4'}$) data for **5**−**7**; 3 $^3J_{HH}$ (see footnote *a*) and 2 $^3J_{HF}$ (i.e., $^3J_{F3''H2''}$ and $^3J_{F3''H4'}$) data for **8**; 3 $^3J_{HH}$ (see footnote *a*) and 2 $^3J_{HF}$ (i.e., $^3J_{F2''H1'}$ and $^3J_{F2''H3'}$) data for **19**; 1 $^3J_{HH}$ ($^3J_{3'4'}$) and 4 $^3J_{HF}$ (see footnote *b*) data for **20**−**23**.

Conclusions

(1) A new seven-parameter Karplus-type relation between vicinal proton−fluorine coupling constants and the corresponding H−C−C−F torsion angles has been proposed. The optimum values of seven parameters were determined with the use of a data set consisting of 57 $^3J_{HF}$ values and the corresponding Φ_{HF} torsion angles, the four substituent λ electronegativities along H−C−C−F fragment, and F−C−C and H−C−C bond angles. The least-squares fit is characterized by the difference between input and back-calculated $^3J_{HF}$ below 2.9 Hz with the overall rms deviation of 1.38 Hz. Our data set of $^3J_{HF}$ values and the corresponding Φ_{HF} torsion angles has been obtained via the conformational analysis of temperature-dependent $^3J_{HH}$ of monofluorinated nucleosides **1**−**11** and has been complemented with the data on the conformationally fixed compounds.

(2) Our new Karplus-type equation has been used to explore the pseudorotational equilibria of monoflurinated nucleosides **24**−**25** as well as difluorinated nucleosides **26**−**29** with the use of both $^3J_{HH}$ and $^3J_{HF}$ coupling constants. The use of temperature-dependent $^3J_{HF}$ in combination with $^3J_{HH}$ for the conformational analysis of fluorinated sugar moieties of nucleosides greatly

facilitated the conformational analysis because the number of experimental data points is greatly increased and the pseudorotational parameters P and Ψ_m of the two interconverting confomers can be better defined. The difluorinated nucleosides **26**−**29** are anticancer compounds, and their solution conformational equilibrium assessed with the use of $^3J_{HF}$ in combination with $^3J_{HH}$ showed a preference of 78−94% (61° < P < 76° and 35° < Ψ_m < 46°) for the puckering between C4′-*exo* and O4′-*endo*-C4′-*exo* forms.

Our new Karplus-type equation will find its application in the studies of the conformational equilibria, where $^3J_{HF}$ values (with or without $^3J_{HH}$) are available, as well as in the determination of the cisoidal versus transoidal orientation of vicinal proton and fluorine atoms in all known and unknown fluorinated compounds.

Experimental Section

^{1}H NMR Spectroscopy. ^{1}H NMR spectra of about 20 mM D_2O or in $CDCl_3$ solutions of **1**−**3**, **5**−**8**, and **24**−**29** were recorded at 270 MHz (JEOL) at various temperatures between 268 and 363 K. For **4** and **9**−**11**, the temperature-dependent $^3J_{HH}$ and $^3J_{HF}$ data have been taken from ref 13. All spectra have been recorded using 64 K data points for a spectral width of ≈10 ppm. The assignments are based on ^{1}H 1D homonuclear decoupling experiments. The coupling constants have been obtained from a first-order analysis of the spectra.

Conformational Analyses. (i) Initial Determination of the Conformation of the Pentofuranose Moiety in 1−11 using PSEUROT Version 5.4. The initial conformational analyses of **1**−**11** with the use of temperature-dependent $^3J_{HH}$ coupling constants have been performed with the program PSEUROT (version 5.4).[14] The following λ substituent "electronegativities" were used for the substituents on H−C−C−H fragments: λ(C1′) = λ(C4′) = λ(C2′ ribo) = 0.62; λ(C2′ deoxy) = 0.67; λ(C5′) = 0.68; λ(O4′) = 1.27; λ(OH) = 1.26; λ(glycosyl N) = 0.58; and λ(F) = 1.37. The results of these conformational analyses using PSEUROT version 5.4 are compiled in Table 2.

(ii) Conformational Analyses Based on $^3J_{HH}$ and/or $^3J_{HF}$ Data with PSEUROT+JHF Program (See Text, Section E for a Description of the Program). Further conformational analyses of **1**−**11** and **24**−**29** involved the use of temperature-dependent $^3J_{HH}$ and $^3J_{HF}$ coupling constants and have been performed with the program PSEUROT+J_{HF}. The program PSEUROT+J_{HF} is based on PSEUROT (ver. 3B)[14] and is written in Fortran 77 and tested on Silicon Graphics computers. PSEUROT+J_{HF} calculates the best fit of experimental $^3J_{HF}$ and $^3J_{HH}$ coupling constants to the five conformational parameters (P and Ψ_m for both N- and S-type conformers and corresponding mole fractions). The input of the experimental coupling constants can be done in one of three ways: (i) only $^3J_{HH}$ coupling constants, (ii) only $^3J_{HF}$ coupling constants, or (iii) $^3J_{HH}$ and $^3J_{HF}$ coupling constants together. The user in addition supplies the following: (a) a set of 6 (for $^3J_{HH}$) or 7 (for $^3J_{HF}$) parameters for the generalized Karplus equations (one set for each coupling constant); (b) the values of A_F (or A_H) and B_F (or A_H) parameters for each pair of H−F (or H−H) J-coupled nuclei along the bonds in the pentofuranosyl moiety which relate H−C−C−F or H−C−C−H torsion angles to the respective endocyclic torsion angles ν_0 − ν_4; (c) the values for F−C−C and H−C−C bond angles from X-ray crystal structure or ab initio calculations (vide infra); (d) four substituent electronegativities; (e) starting values for the pseudorotational parameters; and finally (f) the mole fraction of the S conformer at each temperature (or solvent) where the experimental data is available. The results of these conformational analyses with PSEUROT+J_{HF} are presented in Table 5.

(iii) The PSEUROT+J_{HF} Program. The PSEUROT+J_{HF} program, without the scaling factor option (see our website for the additional changes to be made in order to allow the choice of a scale factor, see also text, section G(iv)), is based on Altona's original PSEUROT (ver. 3B) program in which the lines in Chart 1 have been changed.

Chart 1

```
line 1:          REAL FASE(15),A(15),B(15),SUB(15,4),J(2,15),PHI(2,15),PARAM(15,9)
line 7:          INTEGER F(50),IW1(50),IW2(50),IW3(50),IDNEWP(15)
line 16:         COMMON PARAM,PIII,SUB,IDNEWP
lines 34-37:     IF (NEWP.EQ.0) GOTO 50
                 IF (NEWP.EQ.1) READ (IR,1029) (PARAM(I,K),K=1,6)
                 IF (NEWP.EQ.2) READ (IR,1029) (PARAM(I,K),K=1,9)
                 IDNEWP(I)=NEWP
line 44:         WRITE (IW,1010) (L,L=1,7)
lines 48-51:     IF (IDNEWP(I).EQ.0) WRITE (IW,1011) NAME(I),(PARAM(I,K),K=1,6)
                 IF (IDNEWP(I).EQ.1) WRITE (IW,1011) NAME(I),(PARAM(I,K),K=1,6)
                 IF (IDNEWP(I).EQ.2) WRITE (IW,1011) NAME(I),(PARAM(I,K),K=1,9)
                 70 CONTINUE
lines 335-337:   1010 FORMAT ('PARAMETERS USED IN KARPLUS EQUATION:'/' ',5X,7(8X,'P',
                       +11),5X,'A(FCC)',5X,'A(HCC)')
                 1011 FORMAT (' ',A6,10F10.2)
line 355:        1029 FORMAT (10F8.0)
line 358:        1032 FORMAT ('*** END OF PROGRAM FLUOROT ***')
line 366-367:    1036 FORMAT ('Compound no.:',I5/'TITLE :',10A8,3X+'program FLUOROT')
line 389:        COMMON PARAM(15,9),PHI(2,15),SUB(15,4),IDNEWP(15)
lines 397-400:   IF (IDNEWP(K).LT.2) GOTO 20
                 HF=PARAM(K,7)*(((PARAM(K,8)+PARAM(K,9))/2)-110)*COSB*COSB
                 CAG=CAG+HF
                 20 CONTINUE
line 404:        COMMON PARAM(15,9),PHI(2,15),SUB(15,4),IDNEWP(15)
line 414:    COMMON PARAM(15,9),PHI(2,15),SUB(15,4),IDNEWP(15)
```

***Ab initio* Calculations.** To derive the sets of A and B parameters (vide supra) that correlate H−C−C−H or H−C−C−F to endocyclic pentofuranose torsions and to get some estimates for the HCC and FCC bond angles in our set of constrained systems **12**−**23**, monofluoronucleosides **1**−**11** and **24**−**25**, and difluoronucleosides **26**−**29**, we have performed a series of ab initio calculations (in the gas phase) with the GAUSSIAN 94[20] program using Silicon Graphics Indigo R4000 computers. For all nucleosides, all internal degrees of freedom were freely optimized with the 3-21G basis set except two endocyclic torsion angles (ν_0 and ν_4) which have been fixed at different values chosen in such way that the whole pseudorotation cycle was covered during 7 calculations for FLT (**1**) (P = 0°, 30°, 70°, 140°, 170°, 200°, and 330° with Ψ_m = 35°), AFLT (**3**), F3AT (**8**), and F2″C (**25**) (P = 0°, 30°, 70°, 130°, 170°, 210°, and 320° with Ψ_m = 35° for **3**, 32° for **8**, and 38° for **25**), F2′ddU (**9**) and F2″ddU (**10**) (P = 0°, 40°, 70°, 140°, 180°, 240°, and 300° with Ψ_m = 35°); 8 calculations for FXA (**5**) (P = 0°, 30°, 70°, 130°, 170°, 210°, 250°, and 320° with Ψ_m = 36°); 6 calculations for F3′ddU (**11**) (P = 0°, 40°, 70°, 140°, 240°, and 300° with Ψ_m = 34°); 5 calculations for F3″ddU (**4**) (P = 0°, 40°, 70°, 140°, and 240° with Ψ_m = 34°); and 4 calculations for diFA (**26**) (P = 0°, 60°, 120°, and 180° with Ψ_m = 35°). The A_F and B_F as well as A_H and B_H parameter sets (see Table 3) were assumed to be identical for (i) FLT5 (**2**) and FLT (**1**); (ii) FXA5 (**6**), FXA25 (**7**), and FXA (**5**); (iii) F3′ddA (**24**) and F3′ddU (**11**); and (iv) diFA (**26**), diFG (**27**), diFT (**28**), and diFC (**29**). The optimized structures of **1**, **3**−**5**, **8**−**11**, **25**, and **26** were used to extract Φ_{HF} (or Φ_{HH}) and the corresponding endocyclic torsions $\nu_0 \cdots \nu_4$ at different phase angle values. The A_F and B_F (and A_H and B_H) sets were obtained from linear regressions of Φ_{HF} versus ν_j data. All resulting straight lines had correlation coefficients above 0.95. The following values have been found: 108.1° < $a_{F3''-C3'-C2'}$ < 112.1°, 106.9° < $a_{F3''-C3'-C4'}$ < 109.4°, 108.6° < $a_{H2'-C2'-C3'}$ < 115.0°, 107.3° < $a_{H2''-C2'-C3'}$ < 112.5°, and 107.6° < $a_{H4'-C4'-C3'}$ < 109.8° for FLT (**1**) and FLT5 (**2**); 107.6° < $a_{F3''-C3'-C2'}$ < 112.1°, 107.4° < $a_{F3''-C3'-C4'}$ < 109.9°, 109.8° < $a_{H2'-C2'-C3'}$ < 115.4°, 106.8° < $a_{H2''-C2'-C3'}$ < 112.9°, and 109.3° < $a_{H4'-C4'-C3'}$ < 111.5° for AFLT (**3**); 109.3° <

$a_{F3''-C3'-C2'}$ < 112.0°, 107.4° < $a_{F3''-C3'-C4'}$ < 109.4°, 108.6° < $a_{H2'-C2'-C3'}$ < 114.7°, 107.6° < $a_{H2''-C2'-C3'}$ < 111.7°, and 107.6° < $a_{H4'-C4'-C3'}$ < 110.1° for F3″ddU (**4**); 108.8° < $a_{F3'-C3'-C2'}$ < 111.2°, 107.9° < $a_{F3'-C3'-C4'}$ < 110.6°, 107.5° < $a_{H2'-C2'-C3'}$ < 115.3°, and 110.9° < $a_{H4'-C4'-C3'}$ < 114.5° for FXA (**5**); 106.6° < $a_{F3''-C3'-C2'}$ < 112.6°, 108.0° < $a_{F3''-C3'-C4'}$ < 110.8°, 107.9° < $a_{H2''-C2'-C3'}$ < 113.1°, and 109.0° < $a_{H4'-C4'-C3'}$ < 112.3° for F3AT (**8**); 107.5° < $a_{F2'-C2'-C1'}$ < 112.8°, 108.9° < $a_{F2'-C2'-C3'}$ < 111.7°, 109.8° < $a_{H1'-C1'-C2'}$ < 112.5°, 106.7° < $a_{H3'-C3'-C2'}$ < 112.5°, and 109.5° < $a_{H3''-C3'-C2'}$ < 113.0° for F2′ddU (**9**); 105.2° < $a_{F2''-C2'-C1'}$ < 110.1°, 106.6° < $a_{F2''-C2'-C3'}$ < 112.0°, 107.7° < $a_{H1'-C1'-C2'}$ < 111.3°, 110.2° < $a_{H3'-C3'-C2'}$ < 112.7°, and 106.8° < $a_{H3''-C3'-C2'}$ < 111.2° for F2″ddU (**10**); 108.7° < $a_{F3'-C3'-C2'}$ < 112.3°, 109.6° < $a_{F3'-C3'-C4'}$ < 110.7°, 107.5° < $a_{H2'-C2'-C3'}$ < 112.5°, 109.2° < $a_{H2''-C2'-C3'}$ < 114.0°, and 107.3° < $a_{H4'-C4'-C3'}$ < 112.4° for F3′ddU (**11**); 104.5° < $a_{F2''-C2'-C1'}$ < 112.5°, 106.4° < $a_{F2''-C2'-C3'}$ < 110.6°, 109.0° < $a_{H1'-C1'-C2'}$ < 112.1°, and 108.9° < $a_{H3'-C3'-C2'}$ < 114.0° for F2″C (**25**); 108.8° < $a_{H1'-C1'-C2'}$ < 110.5°, 110.4° < $a_{F2'-C2'-C1'}$ < 113.5°, 107.4° < $a_{F2''-C2'-C1'}$ < 111.7°, 108.4° < $a_{H3'-C3'-C2'}$ < 112.6°, 110.1° < $a_{F2'-C2'-C3'}$ < 113.7°, and 107.9° < $a_{F2''-C2'-C3'}$ < 112.6° for diFA (**26**). For the conformationally fixed compounds **12**−**23**, we have extracted Φ_{HF} torsion angles and a_{FCC} and a_{HCC} bond angles from their ab initio optimized structures (HF/3-21G). a_{FCC} and a_{HCC} were as follows: a_{F-C-C} = 106.2° and a_{HA-C-C} = 106.1° for $^3J_{AF}$ and a_{F-C-C} = 107.4° and a_{HB-C-C} = 110.7° for $^3J_{BF}$ in **12**; a_{F-C-C} = 112.9° and a_{HA-C-C} = 107.3° for $^3J_{AF}$ and a_{F-C-C} = 111.2° and a_{HB-C-C} = 114.7° for $^3J_{BF}$ in **13**; a_{FA-C-C} = 114.3° and a_{HA-C-C} = 111.9° for $^3J_{HAFA}$ and a_{FB-C-C} = 109.5° and a_{HB-C-C} = 108.2° for $^3J_{HBFB}$ in **14**; a_{FA-C-C} = 111.9° and a_{HA-C-C} = 114.3° for $^3J_{HAFA}$, a_{FB-C-C} = 109.5° and a_{HA-C-C} = 114.3° for $^3J_{HAFB}$, a_{FA-C-C} = 111.9° and a_{HB-C-C} = 108.2° for $^3J_{HBFA}$ and a_{FB-C-C} = 109.5° and a_{HB-C-C} = 108.2° for $^3J_{HBFB}$ in **15**; a_{FA-C-C} = 114.3° and a_{HA-C-C} = 111.9° for $^3J_{HAFA}$ and a_{FB-C-C} = 108.2° and a_{HA-C-C} = 111.9° for $^3J_{HAFB}$ in **16**; a_{F2-C-C} = 114.5° and a_{H4-C-C} = 113.4° for $^3J_{H4F2}$ in **17**; a_{F-C-C} = 103.7° and a_{H-C-C} = 112.5° for $^3J_{H2axF}$, a_{F-C-C} = 107.8° and a_{H-C-C} = 109.1° for $^3J_{H4axF}$, a_{F-C-C} = 103.7° and a_{H-C-C} = 111.7° for $^3J_{H2eqF}$, and a_{F-C-C} = 107.8° and a_{H-C-C} = 109.5° for $^3J_{H4eqF}$ in **18**; a_{F-C-C} = 105.4° and a_{H-C-C} = 112.1° for $^3J_{H2axF}$; a_{F-C-C} = 107.7° and a_{H-C-C} = 109.3° for $^3J_{H4axF}$, a_{F-C-C} = 105.4° and a_{H-C-C} = 111.6° for $^3J_{H2eqF}$, and a_{F-C-C} = 107.7° and a_{H-C-C} = 108.5° for $^3J_{H4eqF}$ in **19**; a_{F-C-C} = 107.2° and a_{H-C-C} = 109.7° for $^3J_{H4axF}$ and a_{F-C-C} = 105.0° and a_{H-C-C} = 111.8° for $^3J_{H6axF}$ in **20**; a_{F-C-C} = 107.6° and a_{H-C-C} = 107.3° for $^3J_{H2axF}$, a_{F-C-C} = 106.0° and a_{H-C-C} = 108.7° for $^3J_{H4axF}$, a_{F-C-C} = 107.6° and a_{H-C-C} = 108.1° for $^3J_{H2eqF}$, and a_{F-C-C} = 106.0° and a_{H-C-C} = 107.3° for $^3J_{H4eqF}$ in **21**; a_{F-C-C} = 106.7° and a_{H-C-C} = 108.2° for $^3J_{HaxF}$ in **22**; a_{F-C-C} = 107.7° and a_{H-C-C} = 107.9° for $^3J_{HBF}$ and a_{F-C-C} = 104.1° and a_{H-C-C} = 110.1° for $^3J_{HAF}$ in **23**. It can be seen from the perusal of all bond angles of ab initio optimized structures that bond angles are sensitive to the geometry of the pentofuranose moiety (either N, S, W, or E). Therefore, in the construction of our dataset, we have attempted to take into consideration the uncertainty in the values (±2° or 3°) in such a way that the quality of the fit becomes optimal with the bond angle values listed in Table 4 (columns 10 and 11).

Acknowledgment. We thank the Swedish Natural Science Research Council (NFR), the Swedish Board for Technical Development (NUTEK), and the Swedish Engineering Research Council (TFR) for generous financial support. Thanks are due to the Wallenbergstiftelsen, Forskningsrådsnämnden, and University of Uppsala for funds for the purchase of a 500 MHz Bruker AMX NMR spectrometer. J.P. also thanks the Ministry of Science and Technology of the Republic of Slovenia for the financial support. Authors are indebted to Dr. W. Tong for the preparation of monofluorinated nucleosides.

JO980144K